Physics and Astronomy Faculty Publications
and Presentations

College of Sciences

7-23-2021

Upper limits on the isotropic gravitational-wave background from Advanced LIGO and Advanced Virgo's third observing run

R. Abbott

T. D. Abbott

S. Abraham

F. Acernese

Teviet Creighton
The University of Texas Rio Grande Valley

See next page for additional authors

Recommended Citation

Authors

R. Abbott, T. D. Abbott, S. Abraham, F. Acernese, Teviet Creighton, Mario C. Diaz, Soma Mukherjee, Volker Quetschke, Karla E. Ramirez, and W. H. Wang

Upper limits on the isotropic gravitational-wave background from Advanced LIGO and Advanced Virgo's third observing run

R. Abbott *et al.*[*]

(LIGO Scientific Collaboration, Virgo Collaboration, and KAGRA Collaboration)

We report results of a search for an isotropic gravitational-wave background (GWB) using data from Advanced LIGO's and Advanced Virgo's third observing run (O3) combined with upper limits from the earlier O1 and O2 runs. Unlike in previous observing runs in the advanced detector era, we include Virgo in the search for the GWB. The results of the search are consistent with uncorrelated noise, and therefore we place upper limits on the strength of the GWB. We find that the dimensionless energy density $\Omega_{GW} \leq 5.8 \times 10^{-9}$ at the 95% credible level for a flat (frequency-independent) GWB, using a prior which is uniform in the log of the strength of the GWB, with 99% of the sensitivity coming from the band 20–76.6 Hz; $\Omega_{GW}(f) \leq 3.4 \times 10^{-9}$ at 25 Hz for a power-law GWB with a spectral index of $2/3$ (consistent with expectations for compact binary coalescences), in the band 20–90.6 Hz; and $\Omega_{GW}(f) \leq 3.9 \times 10^{-10}$ at 25 Hz for a spectral index of 3, in the band 20–291.6 Hz. These upper limits improve over our previous results by a factor of 6.0 for a flat GWB, 8.8 for a spectral index of $2/3$, and 13.1 for a spectral index of 3. We also search for a GWB arising from scalar and vector modes, which are predicted by alternative theories of gravity; we do not find evidence of these, and place upper limits on the strength of GWBs with these polarizations. We demonstrate that there is no evidence of correlated noise of magnetic origin by performing a Bayesian analysis that allows for the presence of both a GWB and an effective magnetic background arising from geophysical Schumann resonances. We compare our upper limits to a fiducial model for the GWB from the merger of compact binaries, updating the model to use the most recent data-driven population inference from the systems detected during O3a. Finally, we combine our results with observations of individual mergers and show that, at design sensitivity, this joint approach may yield stronger constraints on the merger rate of binary black holes at $z \gtrsim 2$ than can be achieved with individually resolved mergers alone.

I. INTRODUCTION

The gravitational-wave background (hereafter referred to as the GWB or the background) is a superposition of gravitational-wave (GW) sources that is best characterized statistically [1]. There are many possible astrophysical and cosmological contributions to the background, including distant compact binary coalescences (CBCs) that cannot be resolved individually [2–6], core collapse supernovae [7–11], rotating neutron stars [12–19], stellar core collapses [20,21], cosmic strings [22–26], primordial black holes [27–29], superradiance of axion clouds around black holes [30–33], phase transitions in the early universe [34–38], and GWs produced during inflation [39–41] or in a preheating phase at the end of inflation [42,43]. While some sources of the GWB, such as slow roll inflation, have a fundamentally stochastic character, others like the background from CBCs are a superposition of deterministic sources.

The LIGO Scientific Collaboration and Virgo Collaboration have previously placed upper limits on isotropic [44] and anisotropic [45] GWBs using data from the first two observing runs, in the frequency range 20–1726 Hz. The searches were performed by calculating the cross correlation between pairs of detectors. An extension of this method has been applied to searching for a background of non-tensor modes [44,46,47]; see [48,49] for recent reviews. Cross-correlation methods have also been applied to publicly released LIGO data [50] by other groups, who have obtained similar upper limits [51–53]. A new method that does not rely on the cross-correlation technique and targets the background from CBCs was proposed in [54].

In this work we apply the cross-correlation based method used in previous analyses to Advanced LIGO's [55] and Advanced Virgo's [56] first three observing runs (O1, O2, and O3). We do not find evidence for the GWB, and therefore place an upper limit on the strength. Unlike in previous observing runs, in this work we present the headline results using a log uniform prior [57]. We find

two advantages to using a log uniform prior. First, a log uniform prior gives equal weight to different orders of magnitude of the strength of the GWBs, which is appropriate given our current state of knowledge. Second, a log uniform prior is agnostic as to which power we raise the strain data. It is not clear whether one should put a uniform prior on the strain amplitude, or the strength of the GWB, which scales like the square of the strain. On the other hand, the log uniform prior does not depend on the exponent of the strain data. For completeness, we also present results with a uniform prior on the strength of the GWB in Sec. IV. Results with any other prior can be obtained by reweighing the posterior samples available at [58].

There are several new features in our analysis of the O3 data. First, we incorporate Virgo, by cross correlating the three independent baselines in the LIGO-Virgo network and combining them in an optimal way [59]. Second, in order to handle a large rate of loud glitches in O3, we analyze data where these artifacts have been removed via gating [60,61]. Third, we perform a careful analysis of correlated magnetic noise that could impact the search. In addition to constructing a correlated magnetic noise budget, as in past runs, we use a Bayesian statistical framework developed in [62] to constrain the presence of magnetic noise.

Perhaps the most interesting source of an astrophysical GWB, given the current network sensitivity, is the GWB from CBCs. Previous studies have shown that this GWB may be detectable with Advanced LIGO and Advanced Virgo running at design sensitivity [63,64], and the ability to detect such a background has been confirmed with mock data challenges [65–67]. Therefore in this work we carefully consider the implications of our results for the CBC population. We estimate the GWB using the most up-to-date information from observations during O3 [68–73] and compare with the sensitivity of the current and future detector networks. We show that an upgrade of the current Advanced LIGO facilities, known as A+ [74], could dig into a substantial part of the expected parameter space for the GWB at its target sensitivity. Furthermore, we apply the methods of [75] to constrain the merger rate as a function of redshift for binary black holes (BBHs) by combining the GWB upper limits with information about individually resolvable events. We find that the cross-correlation analysis can provide complementary information at large redshifts, compared to the population analysis using individually detectable events alone [76]. We make the results of our cross correlation analysis available [58], enabling further detailed studies of the GWB from CBCs and other models.

The rest of this work is organized as follows. In Sec. II, we review the method of the cross-correlation search. We discuss the data quality procedures and studies we performed in Sec. III. We present the main results of the search in Sec. IV: we derive upper limits on the GWB in Sec. IV A,

put constraints on the presence of scalar-and vector-polarized backgrounds in Sec. IV B, and in Sec. IV C we extend these results by simultaneously fitting for an astrophysical GWB and an effective GWB arising from magnetic correlations of terrestrial origin. We compare our upper limits with a fiducial model for the GWB from CBCs in Sec. V A, and derive constraints on the BBH merger rate using the upper limits on the GWB and observations of individual CBCs in Sec. V B. We conclude in Sec. VI.

II. METHODS

A GWB that is Gaussian, isotropic, unpolarized, and stationary is fully characterized by a spectral energy density. It is standard to express the spectrum in terms of the dimensionless quantity $\Omega_{\rm GW}(f)$, which is the GW energy density $d\rho_{\rm GW}$ contained in the frequency interval f to $f + df$, multiplied by the GW frequency and divided by df times the critical energy density ρ_c needed to have a flat Universe

$$\Omega_{\rm GW}(f) = \frac{f}{\rho_c}\frac{d\rho_{\rm GW}}{df}, \tag{1}$$

where $\rho_c = 3H_0^2 c^2/(8\pi G)$, c is the speed of light, and G is Newton's constant. For consistency with other GW measurements (for example those of [68]), we take the Hubble constant from Planck 2015 observations to be $H_0 = 67.9~{\rm km\,s^{-1}\,Mpc^{-1}}$ [77].

A. Cross correlation spectra

Let us label the GW detectors in the LIGO-Hanford, LIGO-Livingston, and Virgo (HLV) network by the index $I = \{H, L, V\}$. We denote the time-series output of the detectors by $s_I(t)$, and the Fourier transform by $\tilde{s}_I(f)$. Following [48,59], we define the cross-correlation statistic for the baseline IJ as

$$\hat{C}^{IJ}(f) = \frac{2}{T}\frac{{\rm Re}[\tilde{s}_I^\star(f)\tilde{s}_J(f)]}{\gamma_{IJ}(f)S_0(f)}, \tag{2}$$

where $\gamma_{IJ}(f)$ is the normalized overlap reduction function [59,78,79] for the baseline IJ, the function $S_0(f)$ is given by $S_0(f) = (3H_0^2)/(10\pi^2 f^3)$, and T is the observation time. In practice, because the noise is nonstationary, we break the data into segments, and then take T to be the segment duration. We then average together segments using inverse noise weighting [59]. If the noise were stationary, this average would reproduce Eq. (2). This estimator is normalized so that $\langle \hat{C}^{IJ}(f) \rangle = \Omega_{\rm GW}(f)$ in the absence of correlated noise. In the small signal-to-noise ratio limit, the variance can be estimated as

$$\sigma_{IJ}^2(f) \approx \frac{1}{2T\Delta f}\frac{P_I(f)P_J(f)}{\gamma_{IJ}^2(f)S_0^2(f)}, \tag{3}$$

where Δf is the frequency resolution, and $P_I(f)$ is the one-sided power spectral density in detector I. Note that $T\Delta f$ need not equal one if several frequency bins are coarse grained around the central frequency f to produce the estimator in Eq. (2).

While we have expressed the cross-correlation estimator in terms of the GW strain channel, in fact this analysis can be applied to *any* pair of instruments. Following [62], in Sec. III D and Sec. IV C we will also employ these techniques to cross correlate magnetometer channels to search for correlated magnetic noise.

B. Optimal filtering

Strictly speaking, the optimal estimator for a given signal includes both autocorrelation and cross-correlation terms [48]. We only use the cross correlation, and not autocorrelation, in the search because the noise power spectral density is not known precisely enough to be subtracted accurately, and therefore in practice the cross correlation is nearly optimal. With this caveat, we can construct an optimal estimator to search for a GWB of any spectral shape by combining the cross-correlation spectra from different frequency bins with appropriate weights

$$\hat{C}^{IJ} = \frac{\sum_k w(f_k)\hat{C}^{IJ}(f_k)\sigma_{IJ}^{-2}(f_k)}{\sum_k w(f_k)^2\sigma_{IJ}^{-2}(f_k)},$$
$$\sigma_{IJ}^{-2} = \sum_k w(f_k)^2\sigma_{IJ}^{-2}(f_k), \quad (4)$$

where f_k are a discrete set of frequencies, and the optimal weights for spectral shape $\Omega_{\mathrm{GW}}(f)$ are given by

$$w(f) = \frac{\Omega_{\mathrm{GW}}(f)}{\Omega_{\mathrm{GW}}(f_{\mathrm{ref}})}. \quad (5)$$

Here, f_{ref} is a fixed reference frequency. For ease of comparison with previous observing runs, we choose the reference frequency to be $f_{\mathrm{ref}} = 25$ Hz. This is approximately the start of the most sensitive frequency band for the isotropic search as described in [44]. This analysis is very flexible and can be applied to a GWB of any spectral shape. We will report results for a power law GWB of the form

$$\Omega_{\mathrm{GW}}(f) = \Omega_{\mathrm{ref}}\left(\frac{f}{f_{\mathrm{ref}}}\right)^{\alpha}. \quad (6)$$

Our final estimator combines information from all baselines optimally using the sum

$$\hat{C} = \frac{\sum_{IJ}\hat{C}^{IJ}\sigma_{IJ}^{-2}}{\sum_{IJ}\sigma_{IJ}^{-2}}, \qquad \sigma^{-2} = \sum_{IJ}\sigma_{IJ}^{-2}, \quad (7)$$

where $\sum_{IJ}$ is a shorthand notation meaning a sum over all *independent* baselines IJ. We can also include

cross correlation results from previous observing runs in a natural way by including them in this sum as separate baselines. More concretely, we combine HL-O1, HL-O2, HL-O3, HV-O3, and LV-O3.

C. Parameter estimation

In order to estimate parameters of a specific model of the GWB, we combine the spectra from each baseline IJ to form the likelihood [80]

$$p(\hat{C}_k^{IJ}|\boldsymbol{\Theta}) \propto \exp\left[-\frac{1}{2}\sum_{IJ}\sum_k\left(\frac{\hat{C}_k^{IJ} - \Omega_{\mathrm{M}}(f_k|\boldsymbol{\Theta})}{\sigma_{IJ}(f_k)}\right)^2\right], \quad (8)$$

where $\hat{C}_k^{IJ} \equiv \hat{C}^{IJ}(f_k)$, and where we assume that the $\hat{C}_k^{IJ}$ are Gaussian-distributed in the absence of a signal. The term $\Omega_{\mathrm{M}}(f|\boldsymbol{\Theta})$ describes the model for the GWB, characterized by the set of parameters $\boldsymbol{\Theta}$. This hybrid frequentist-Bayesian approach has been shown to be equivalent to a fully Bayesian analysis in [81].

Equation (8) assumes that cross-correlation spectra measured between different baselines are uncorrelated. This is not strictly true, as different baselines share detectors in common. Correlations between baselines, however, enter at $\mathcal{O}(\Omega^2)$ and so can be neglected in the small-signal limit [59].

In this work we shall consider several different models:

(i) *Noise* (N): $\Omega_{\mathrm{N}}(f) = 0$. We implicitly include uncorrelated Gaussian noise as part of every model that follows.

(ii) *Power law* (PL): $\Omega_{\mathrm{PL}}(f) = \Omega_{\mathrm{ref}}(\frac{f}{f_{\mathrm{ref}}})^{\alpha}$. The parameters Θ_{PL} are the amplitude Ω_{ref} and spectral index α. We will consider cases in which α is allowed to vary as well as those in which it is fixed.

(iii) *Scalar-vector-tensor power law* (SVT-PL): This model contains tensor polarizations, as allowed in general relativity (GR), and vector and scalar polarizations, which are forbidden in GR but generically appear in alternative theories of gravity. We define p to be an index referring to polarization, $p = \{T, V, S\}$, where T, V, and S refer to tensor, vector, and scalar polarized GWs, respectively. We assume the GWB for each polarization can be described by a power law, which may be different for each polarization. Thus there are six parameters $\Theta_{\mathrm{SVT-PL}}$, given by the amplitudes $\Omega_{\mathrm{ref}}^{(\mathrm{p})}$ and spectral indices α_{p} for each polarization. The model is given by the sum $\Omega_{\mathrm{SVT-PL}}(f) = \sum_{\mathrm{p}}\beta_{IJ}^{(\mathrm{p})}(f)\Omega_{\mathrm{ref}}^{(\mathrm{p})}(\frac{f}{f_{\mathrm{ref}}})^{\alpha_{\mathrm{p}}}$, where $\beta_{IJ}^{(\mathrm{p})}(f) = \gamma_{IJ}^{(\mathrm{p})}(f)/\gamma_{IJ}(f)$ is the ratio of the overlap reduction function for polarization p and baseline IJ to the standard (tensor) overlap reduction function for that baseline [46].

(iv) *Magnetic* (MAG): $\Omega_{\mathrm{MAG}}(f)$ describes correlations between two detectors induced by large-scale

coherent magnetic fields, which can appear as an *effective* background. We model this effective background in terms of magnetometer correlations and a transfer function between the local magnetic field and the strain channel of the detectors. The free parameters $\mathbf{\Theta}_{\mathrm{MAG}}$ describe the coupling function, as described in Sec. IV C.

(v) *CBC*: $\Omega_{\mathrm{CBC}}(f)$ is determined by an underlying parametrized model for the mass distribution of compact binaries and their merger rate $R(z)$ as a function of redshift. The parameters of this model are discussed in Sec. V.

We will also consider combinations of these models, for example $\Omega_{\mathrm{M}}(f) = \Omega_{\mathrm{PL}}(f) + \Omega_{\mathrm{MAG}}(f)$. Given the likelihood, we form a posterior using Bayes theorem, $p(\mathbf{\Theta}|C_k^{IJ}) \propto p(C_k^{IJ}|\mathbf{\Theta})p(\mathbf{\Theta})$, where $p(\mathbf{\Theta})$ is the prior distribution on the parameters $\mathbf{\Theta}$. We will consider different prior choices for each model we consider below.

Finally, it is often of interest to combine upper limits on the amplitude of the GWB with other observations, in order to obtain the best possible constraints on a given model. For example, such a strategy can be used to combine measurements across a range of frequency bands as in [82]. Denoting data from the other observations as $\hat{D}$, we can consider a factorized likelihood

$$p(\hat{C}^{IJ}(f_k), \hat{D}|\mathbf{\Theta}) = p(\hat{C}^{IJ}(f_k)|\mathbf{\Theta})p(\hat{D}|\mathbf{\Theta}). \qquad (9)$$

In Sec. V B, we will apply this method to combine the upper limits on the GWB with observations of individual BBH events from [68], similar to that performed in [75].

III. DATA QUALITY

A. Data

We analyze strain data taken during O3 by the LIGO-Hanford, LIGO-Livingston, and Virgo detectors. The O3 run is divided into two sets. The first, O3a, began April 1, 2019, 15:00 UTC, and continued until October 1, 2019 15:00 UTC, while O3b ran from November 1 2019, 15:00 UTC, to March 27, 2020 17:00 UTC. The HL baseline had 205.4 days of coincident livetime, HV 187.5 days, and LV 195.4 days, before applying any data quality vetoes.

We look for correlated magnetic noise using magnetometers located at the sites. Each LIGO detector has installed two low-noise LEMI-120 magnetometers [83]. The Virgo detector has two low-noise MFS-06 magnetometers by Metronix [84]. In order to allow a comparison between the magnetic and GW searches, we apply the same data processing to the magnetometer channels that we do to the strain channels, except where otherwise stated.

The data are first downsampled. For the GW data, we decimate the data from the original sampling rate 16384 Hz to 4096 Hz. The maximum frequency that we analyze is 1726 Hz, which is sufficiently below the Nyquist frequency

to avoid aliasing effects. Since we only analyze magnetic data up to 100 Hz, we downsample the LEMI magnetometers from 16384 Hz to 512 Hz, and the Metronix magnetometers from 2000 Hz to 512 Hz. Then the data are high-pass filtered using a 16th-order Butterworth filter with a knee frequency of 11 Hz, which is constructed using second-order sections. We divide the original data stream into time segments of duration 192 s which are Hann-windowed and overlapped by 50%, then compute a discrete Fourier transform on each of these segments, and coarse-grain the resulting spectrum to a frequency resolution of 1/32 Hz. We perform the cross-correlation search with a publicly available implementation [85] of the algorithm described in Sec. II using MATLAB [86].

As an end-to-end test of the entire system, we added stochastic signals in the Hanford and Livingston detectors by actuating the test masses, following the procedures described in [87]. We injected the same realization of the stochastic background with a flat power law index and strength of 4.3×10^{-5} in two 15-minute segments of data. We found for the first injection $\Omega_{\mathrm{GW}} = (4.6 \pm 0.4) \times 10^{-5}$ and the second $\Omega_{\mathrm{GW}} = (4.7 \pm 0.4) \times 10^{-5}$; both recoveries are statistically consistent with the injected signal.

B. Time and frequency domain cuts

For each baseline, we require that both detectors in the baseline are in observing mode, and that there are no critical issues with the detector hardware, as defined by category 1 vetoes described in [88,89]. As in previous runs, we apply a nonstationarity cut by removing times where the square root of the variance in Eq. (4) is found to vary by more than 20% between segments. We take the union of the cuts for $\alpha = \{-5, 0, 3, 5\}$; each power law is sensitive to a different frequency band. While we use $\alpha = 2/3$ for the search, we do not include it in the cut since it does not provide significantly new information for the nonstationarity cut, because the frequency range is very similar to the one probed by $\alpha = 0$. We remove Hanford data from April 1–April 16 2019 due to nonstationarity arising from calibration lines at 35.9 and 36.7 Hz. These lines were moved below 20 Hz on April 16, 2019.

In principle, the CBC signals known to be present in the data contribute to the integrated cross-correlation. Using the median values for the masses and redshifts of direct detections in O3a [68], the livetime for O3a, and the inspiral approximation in Eq. 16 of [67], we estimate that resolved sources contribute $\Omega_{\mathrm{GW}} \lesssim 10^{-10}$ to the GWB, which is well below the O3 sensitivity. Therefore we do not remove the observed CBCs from the data.

After applying the category 1 vetoes and nonstationarity cut, we found that 17.9% of available livetime was lost in the HL baseline, 22.1% in the HV baseline, and 21.9% in the LV baseline.
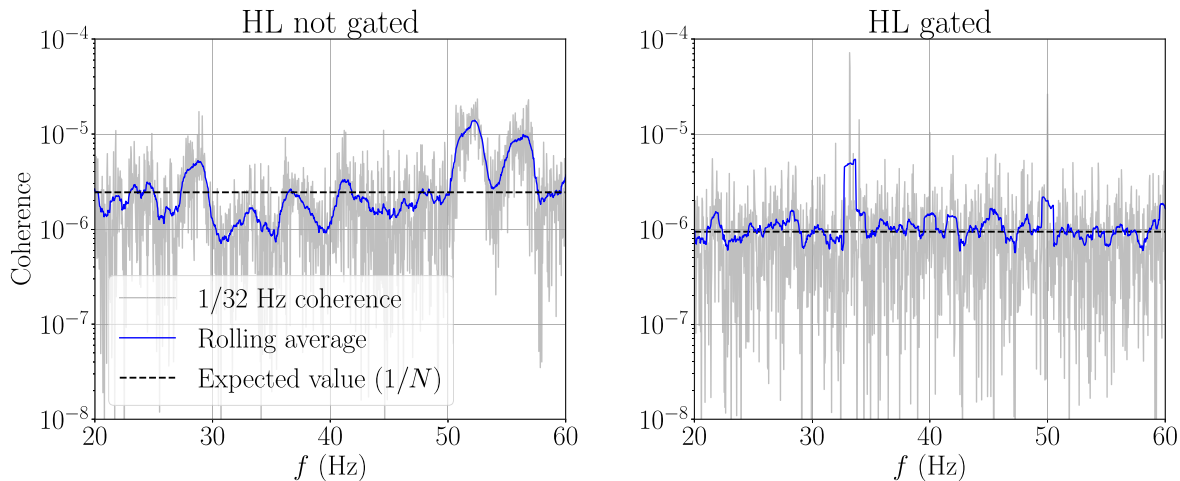
FIG. 1. Coherence spectra for the HL baseline without (left panel) and with (right panel) gating applied. In both cases, we have applied the nonstationarity cut described in the main text. We show the coherence spectrum at 1/32 Hz (the same frequency resolution used for the isotropic search) as a gray line, a rolling average with a 1 Hz resolution as a blue line, and the average value expected for uncorrelated, Gaussian noise which is given by 1 divided by the number of averages used to make the coherence spectrum as a black dashed line. The gated coherence is consistent with the expectation from Gaussian noise, while the spectrum without gating is not. Additionally, we see that more segments are used for averages in the gated spectrum after applying the nonstationarity cut described in the text. This is because without gating, many segments are removed due to a single glitch biasing the power spectrum estimate of the segment. Note that in this figure, we have not applied any frequency notching; the large line visible at 33.2 Hz is due to a beat note in the calibration lines at both H1 and L1 arising from nonlinear couplings.

We do not analyze frequency bins where there is evidence of coherence between instruments that is determined to be caused by the instruments themselves. The coherence between two channels,

$$\Gamma_{IJ}(f) = \frac{\langle|\tilde{s}_I^\star(f)\tilde{s}_J(f)|^2\rangle}{\langle|\tilde{s}_I(f)|^2\rangle\langle|\tilde{s}_J(f)|^2\rangle}, \tag{10}$$

is a useful measure to determine when correlations in a given frequency bin exceed what is expected from uncorrelated data. In the above expression, the angle brackets $\langle\rangle$ refer to an average over analysis segments. The coherence between the strain and auxiliary channels at a given site can also be used to identify an instrumental source of contamination [90]. We removed 13.3% of the frequency band in the HL baseline, 21.5% of the frequency band in the HV baseline, and 18.9% of the frequency band in the LV baseline. However, we only removed 3.2% from HL, 9.3% from HV, and 5.9% from LV below 300 Hz, where the search is most sensitive. In O3, we found many 1 Hz harmonics which were coherent between Hanford and Virgo. We also observed a large coherent line in the HL baseline at 33.2 Hz, which was likely due to the beating of two different calibration lines at Hanford and Livingston, and therefore did not appear in linear coherences between the strain and auxiliary channels. Generally speaking, line mitigation efforts were particularly effective at the LIGO-Livingston detector, and the HL and LV baselines had many fewer coherent lines. The full list of frequencies removed from the analysis is available online [58].

C. Gating

In O3, we found a much higher rate of loud glitches compared to previous observing runs [89]. A naive application of the standard nonstationarity cut used in previous searches led to losing >50% of the data when running with 192-s data segments. In order to reduce the amount of data lost to the nonstationarity cut, and thus improve the sensitivity of the search, we pre-conditioned the data by applying a gating procedure. This procedure involves first identifying data from the Hanford and Livingston baselines that contain a glitch, and then zeroing out these data. We defined segments containing a glitch when the root-mean-squre (RMS) value of the whitened strain channel in the 25–50 Hz band or 70–110 Hz band exceeded a threshold value. We then removed the glitches from the time series by multilpying the data in these segments by an inverse Tukey window. We found that a total of 0.4% of Hanford data was gated in the data that we analyzed, and 1% of Livingston data for each baseline. We refer the interested reader to [60] for further details of the procedure, including the whitened channels and precise thresholds used. This was not necessary for Virgo data due to the lower rate of large glitches. The impact of gating can be clearly seen on the coherence spectra, as we show in Fig. 1. Compared to the nongated data, many more segments are analyzed after applying nonstationarity cuts, and the spectrum is much closer to what is expected from uncorrelated Gaussian noise. It was discovered that from April 20–25 a 1/120-Hz comb was visible in the Livingston data around large calibration lines.

The comb was caused by an inadvertently running diagnostic camera clicking at regular two minute intervals. To be cautious, we removed this period of time from the analysis. We have verified with a mock data challenge that applying this gating procedure to simulated data did not affect our ability to recover a GWB. This check is described further in [61].

D. Correlated magnetic noise budget

In order to be able to claim detection of a GWB, one must understand and control environmental sources of correlated noise [91]. Some magnetic fields are expected to be correlated between sites and are monitored with sensitive magnetometers placed away from the buildings. For example, Schumann resonances are electromagnetic modes of the Earth-ionosphere resonant cavity [92]. They are coherent on a global scale [93], so if they couple to the interferometer and produce noise in the GW channel, they will cause correlations between the outputs of detectors on different continents [94,95]. If these effects are large enough, they can be a source of confusion noise for cross-correlation searches. In this section we show that there is no evidence for correlated magnetic noise in the O3 GW strain data.

As in past runs [44,96], following [94,95] we create a budget for the magnetic correlations

$$\hat{C}_{\text{mag},IJ}(f) = \frac{2}{T} \frac{|T_I(f)||T_J(f)|\text{Re}[\tilde{m}_I^\star(f)\tilde{m}_J(f)]}{\gamma_{IJ}(f)S_0(f)}, \quad (11)$$

where $\tilde{m}_I(f)$ are Fourier transforms of the magnetometer channels. The coupling functions $T_I(f)$ are estimated by injecting an oscillating magnetic field of a known frequency and amplitude at different locations near each detector, and measuring the resulting output in the GW strain channel. Weekly injections were performed to study the time-dependence of the magnetic coupling [97].

Potential differences in the strength of the magnetic field at the magnetometers located around the detector versus the strength of the field at the "true" coupling location mean that these measurements are only rough estimates, and are susceptible to large uncertainties. This uncertainty is estimated by comparing injections at different locations at each site; to account for this, we include a factor of two uncertainty in the coupling function of each detector [98].

Another possible source of error in the coupling function measurement is that the low-noise magnetometers are located outside, far from the local magnetic noise associated with the buildings, but the weekly injections described above are performed inside. One may worry that ferromagnetic material in the buildings can amplify the outside-to-inside magnetic coupling. However, additional measurements at Handford suggest that the coupling function from outside to inside the building is less

than one. Injections were performed around the corner station using seven frequencies ranging from 11 to 444 Hz, and the magnetic field was measured inside and outside the building at the same distance from the injection coil. A power-law fit to the ratio of the magnetic field measured inside to the field measured outside as a function of frequency indicates that the magnetic coupling is suppressed by up to a factor of 2 in the frequency range 10–100 Hz, however with variation depending on the orientation of the field. To be conservative, we assume the inside-to-outside magnetic coupling is equal to one.

To construct the budget, we first compute a linear interpolation for the coupling function as a function of frequency measured at each detector in each week. For weeks where a coupling function was not measured, we use the coupling function that was nearest in time. For each baseline, and each week, we then multiply the coupling functions for each detector by the magnetic cross-correlation spectrum for that baseline, to form a budget. We use the pair of directions that gives the largest coherence. Studies based on shorter stretches of data indicate that the coherence of the magnitude of the magnetic field can be up to a factor of two larger than the coherence of the worst-case components; therefore to be conservative we multiply the coherence in each detector baseline by a factor of two. We combine the budgets across baselines by using the error bars from the GW channels as weights to account for the relative sensitivity of each baseline, $\hat{C}_{\text{mag}} = \sum_{IJ} w_{IJ}(f)\hat{C}_{\text{mag},IJ}(f)$, where $w_{IJ}(f) = (\sigma_{IJ}(f)/\sigma(f))^{-2}$. We show an estimate of the correlated magnetic noise compared to the O3 sensitivity curve in Fig. 2, combining all three baselines. The red band shows the range of budgets we obtain accounting for the combined weekly magnetic coupling function measurements, as well as the overall factor of two uncertainty in each detector's coupling function described above. The overall trend of the red band should be compared with the O3 power-law integrated (PI) curve [99], which shows the sensitivity of our search to power law backgrounds, accounting for integration over frequency. The black dotted line shows the upper range of the budget. Narrowband features should be compared with $\sigma(f)$, shown as a black solid line, which shows the sensitivity to a GWB in every frequency bin. The measurements at Hanford were sampled at a fine frequency resolution due to the use of broadband injections with a large coil [100]. This allowed us to see fine-grained features in the coupling function, such as the broad resonances visible between 80 Hz and 100 Hz Fig. 2. While the exact origin of these resonances is presently unknown, they are correlated with excess motion of test masses in the power recycling cavity [101]. The final budget indicates that the nonobservation of correlated magnetic noise is expected given the coupling function measurements.
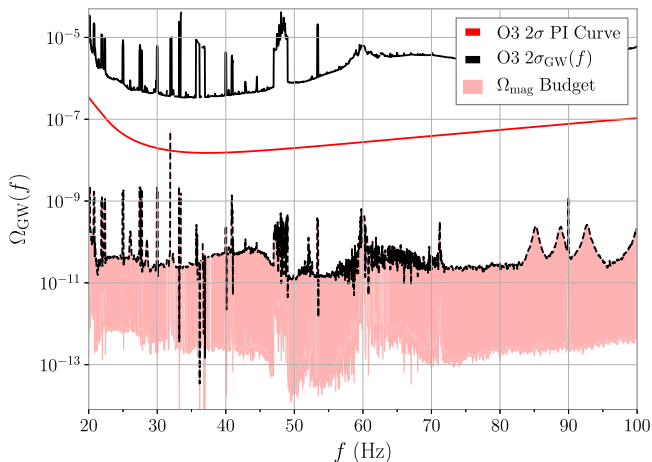
FIG. 2. Correlated magnetic noise budget, as described in the main text. The band shows the expected range of magnetic contamination, using weekly measurements of the coupling function at each site, and accounting for the uncertainty in the coupling function measurements. We display the O3 sensitivity in two ways. First, we plot the power-law integrated (PI) curve as a red line. This indicates the sensitivity of the search to power-law backgrounds and includes the effect of integrating over frequencies, and should be compared with the overall trend of the red band. Second, we plot the square root of the variance, $\sigma(f)$, as a black line, which gives the sensitivity of the search to narrowband features. This can be compared with narrow features in the upper range of the noise budget, which we show as a black dashed line. We conclude that the O3 sensitivity is well above the level of correlated magnetic noise estimated in O3.

IV. RESULTS

A. Upper limits on the GWB

In Table I we report the point estimate and 1-σ error bar from O3 obtained from each baseline independently, as well as combining all three baselines together with the HL baseline results available from O1 and O2, using an optimal filter for three different power law models

(i) $\alpha = 0$ approximately characterizes cosmic string [22–26], and slow-roll inflation GWBs [39–41] in the LIGO-Virgo frequency band.

(ii) $\alpha = 2/3$ describes the CBC GWB when contributions from the inspiral dominate the GWB, which is a very good approximation in the LIGO-Virgo frequency band [102]. However, this approximation may not be valid for mergers of binaries arising from Population III stars [103], or from heavy BBH mergers with masses above the pair-instability mass gap [104].

(iii) $\alpha = 3$ is a fiducial choice used in past searches which approximately describes some astrophysical sources such as supernovae [10–37,39–88,90,92–105], and corresponds to a GWB that is flat in the strain power, $S_h(f) \propto f^{-3}\Omega_{\mathrm{GW}}(f)$ [59].

While we use the entire band 20–1726 Hz to compute the point estimate and error bar, we also show $f_{99\%}^{IJ}$, which is the upper frequency of the band starting at 20 Hz that contains 99% of the sensitivity in baseline IJ.

The HL baseline contributes most to the sensitivity. The contributions from the baselines that include Virgo are relatively more important at higher frequencies and especially relevant to searches for larger power laws. We note that the point estimates for HV and LV are approximately 2σ away from zero, however we do not interpret this as evidence of a signal given that the point estimate of the much more sensitive HL baseline is consistent with zero to within 1σ. The combined spectrum is shown in Fig. 3. From this figure, one can see that the point estimate fluctuates roughly symmetrically around zero, consistent with expectations from Gaussian noise. Additionally, by comparing with Fig. 1 of [44], it is clear that the addition of Virgo data compensates for a zero in the HL overlap reduction function at around 64 Hz. After having applied the data quality cuts described in Sec. III, data are consistent with uncorrelated, Gaussian noise. The spectra have a χ^2-per-degree-of-freedom value of 0.98.

Since we do not find evidence of a GWB, we place upper limits on the PL model, combining the O3 spectra with the results from previous runs. We report upper limits using both a prior that is uniform in the log of the strength of the GWB, and a prior that is uniform in the strength. We choose to report the upper limit obtained with the log uniform prior as our headline result, because a log uniform prior is a more

TABLE I. Search results for an isotropic GWB, using the optimal filter method for power law GWBs with $\alpha = \{0, 2/3, 3\}$. For each of the three baselines IJ, we show the point estimate and 1σ uncertainty for the cross-correlation estimate C_{IJ}, along with the frequency band from 20 Hz to $f_{99\%}^{IJ}$ containing 99% of the sensitivity. We see that the HL baseline is the most sensitive, and the HV and LV baselines are more sensitive at higher frequencies, and for larger spectral indices, due to the longer baseline. In the last two columns, we also present the search result combining all three baselines from O3, as well as the O1 and O2 data. As noted in the main text, the point estimates for the HV and LV are approximately 2σ away from zero, however this is not consistent with a GWB given the result of the much more sensitive HL baseline.

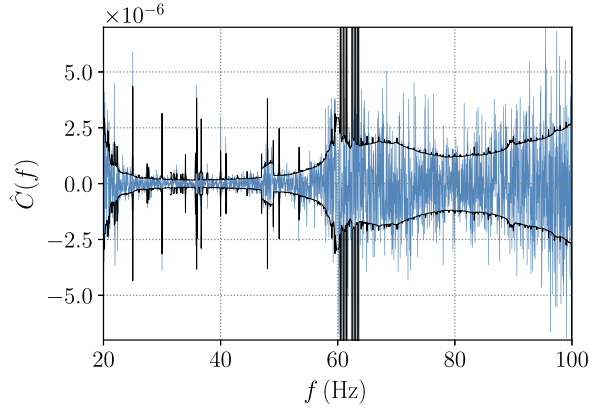| Power law	$f_{99\%}^{\mathrm{HL}}$ [Hz]	$\hat{C}^{\mathrm{HL}}/10^{-9}$	$f_{99\%}^{\mathrm{HV}}$ [Hz]	$\hat{C}^{\mathrm{HV}}/10^{-9}$	$f_{99\%}^{\mathrm{LV}}$ [Hz]	$\hat{C}^{\mathrm{LV}}/10^{-9}$	$f_{99\%}^{\mathrm{O1+O2+O3}}$ [Hz]	$\hat{C}^{\mathrm{O1+O2+O3}}/10^{-9}$
0	76.1	-2.1 ± 8.2	97.7	229 ± 98	88.0	-134 ± 63	76.6	1.1 ± 7.5
2/3	90.2	-3.4 ± 6.1	117.8	145 ± 60	107.3	-82 ± 40	90.6	-0.2 ± 5.6
3	282.8	-1.3 ± 0.9	375.8	9.1 ± 4.1	388.0	-4.9 ± 3.1	291.6	-0.6 ± 0.8

FIG. 3. Cross-correlation spectra combining data from all three baselines in O3, as well as the HL baseline in O1 and O2. As described in the main text, the spectrum is consistent with expectations from uncorrelated, Gaussian noise.

natural choice for a scaling parameter, and also is more sensitive to small signals. However, since upper limits computed with a uniform prior are more conservative, we present results for the uniform prior as well. For both cases, we choose the upper bound of the prior to be large enough that there is no posterior support at the upper end of the prior range. For the log uniform prior, the upper limit depends mildly on the lower bound of the prior range, which cannot be taken to be zero. Following [44], we choose the lower bound to be $\Omega_{\text{ref}} \geq 10^{-13}$. This choice enables a direct comparison with previous upper limits, and is the same order of magnitude as the expected reach of next-generation ground-based detectors [106–108].

For the spectral index, we compute upper limits by fixing α to the three values $\{0, 2/3, 3\}$ discussed earlier, as well as allowing α to vary. For the latter case, we assume a Gaussian prior on α with zero mean and standard deviation 3.5. This prior on α is very similar to the triangular prior on α we used in the O2 analysis [44], however it does not vanish for large values of $|\alpha|$. Therefore in principle, this prior allows us to probe extreme power laws if the data support them. We have checked that the Gaussian prior

gives posterior distributions that are nearly identical to those produced using the triangular prior.

We marginalize over calibration uncertainty following the methods in [109]. We use an amplitude calibration uncertainty of 7.0% for Hanford, 6.4% for Livingston, and 5% for Virgo [110]; this is a conservative choice describing the worst case over the entire run. We use the same amplitude calibration uncertainty factors for O1 and O2 as in previous analyses [44]. In all cases, phase uncertainty is negligible. The results are given in Table II. We also show the posterior in the Ω_{ref}-α plane in Fig. 4.

At the 95% credible level, using a log-uniform (uniform) prior, we find that $\Omega_{\text{GW}}(25 \text{ Hz})$ is less than 5.8×10^{-9} (1.7×10^{-8}) for $\alpha = 0$, 3.4×10^{-9} (1.2×10^{-8}) for $\alpha = 2/3$, 3.9×10^{-10} (1.3×10^{-9}) for $\alpha = 3$, and 6.6×10^{-9} (2.7×10^{-8}) when marginalizing over α. This represents an improvement by a factor of about 6.0 (3.6) for a flat power law, 8.8 (4.0) for a power law of $\alpha = 2/3$, and 13.1 (5.9) for a power law of $\alpha = 3$. The improvement for large α is due in part to the improved high-frequency sensitivity of Advanced LIGO in O3; to the addition of the baselines involving Virgo; and to the specific noise realization, in particular the negative point estimate $\alpha = 3$ in O3, as seen in Table I. We find a $\log_{10}$ Bayes Factor of -0.3 when comparing the hypotheses of signal and noise to noise-only when marginalizing over α.

B. Non-GR polarizations

We can use our results to constrain modifications to GR by using the SVT-PL model defined in Sec. II C. This analysis benefits from the inclusion of Virgo data, since adding more detectors to the network can help distinguish between different polarizations, as shown in [46]. We note that Ω_{GW} does not necessarily have the interpretation of an energy density in modified theories of gravity, and it is in general more appropriate to think of these quantities as a measure of the strain power in each polarization [111].

We use the log-uniform prior on each strength $\Omega_{\text{ref}}^{(p)}$ and the Gaussian prior for each spectral index α_{p}, as described

TABLE II. Upper limits at the 95% credible level on Ω_{ref} under the power law model for the GWB. We show upper limits conditioned on different fixed power law indices α, as well as a marginalized limit obtained by integration over α, using a Gaussian prior with zero mean and a standard deviation of 3.5. We show the results using a prior that is uniform in Ω_{ref}, as well as uniform in $\log \Omega_{\text{ref}}$. As described in the main text, the uniform upper limits are more conservative, while the log uniform priors are more sensitive to weak signals. We also compare with the upper limits from [44], and give the improvement factor we achieve using O3 data.

	Uniform prior			Log-uniform prior		
α	O3	O2 [44]	Improvement	O3	O2 [44]	Improvement
0	1.7×10^{-8}	6.0×10^{-8}	3.6	5.8×10^{-9}	3.5×10^{-8}	6.0
2/3	1.2×10^{-8}	4.8×10^{-8}	4.0	3.4×10^{-9}	3.0×10^{-8}	8.8
3	1.3×10^{-9}	7.9×10^{-9}	5.9	3.9×10^{-10}	5.1×10^{-9}	13.1
Marg.	2.7×10^{-8}	1.1×10^{-7}	4.1	6.6×10^{-9}	3.4×10^{-8}	5.1
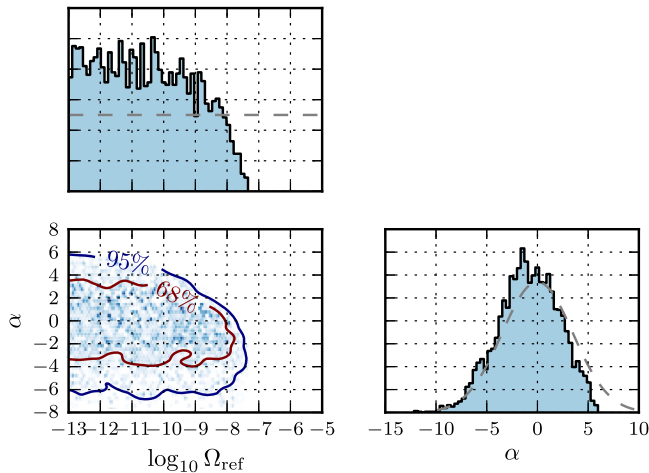
FIG. 4. Posteriors for the strength Ω_{ref} and spectral index α for the power law model described in the main text, using a prior uniform in the log of Ω_{ref}. The top and right panels show marginalized posteriors for Ω_{ref} and α, while the center plot shows the 2D posterior density. The dashed, gray lines indicate the prior distributions.

in the previous section. We show the results in Table III. Marginalizing over the spectral indices for each polarization, we find that the upper limit on a scalar-polarized GWB in this model is $\Omega_{\mathrm{GW}}^{(S)}(25\ \mathrm{Hz}) \leq 2.1 \times 10^{-8}$, the limit on a vector GWB is $\Omega_{\mathrm{GW}}^{(V)}(25\ \mathrm{Hz}) \leq 7.9 \times 10^{-9}$, and the limit on a tensor GWB is $\Omega_{\mathrm{GW}}^{(T)}(25\ \mathrm{Hz}) \leq 6.4 \times 10^{-9}$. Note that the upper limit on tensor modes in this analysis is slightly different from the upper limit when we consider only GR modes given in the previous section, because of the inclusion of additional parameters under this current model.

We compute two Bayesian odds ratios $\mathcal{O}$: the odds $\mathcal{O}_{\mathrm{N}}^{\mathrm{SIG}}$ that a stochastic background of *any* polarization is present (SIG) versus Gaussian noise (N), and the odds $\mathcal{O}_{\mathrm{GR}}^{\mathrm{NGR}}$ that alternative polarization modes are present (NGR) versus standard tensor polarizations obeying GR. Note that the signal hypothesis is formally the union of seven distinct sub-hypotheses, corresponding to the seven possible combinations of tensor, vector, and scalar modes (T, TV, TS, TVS, etc.) When computing $\mathcal{O}_{\mathrm{N}}^{\mathrm{SIG}}$, we adopt equal prior odds between the signal and noise hypotheses, and within

the signal hypothesis assign equal priors among the various signal subhypotheses. Similarly, in computing $\mathcal{O}_{\mathrm{GR}}^{\mathrm{NGR}}$ we choose equal priors between NGR and GR hypotheses, and within NGR assign equal priors to the six distinct ways that nonstandard polarizations might be present; see Refs. [46] and [47] for more details. We find $\log_{10}\mathcal{O}_{\mathrm{N}}^{\mathrm{SIG}} = -0.4$ and $\log_{10}\mathcal{O}_{\mathrm{GR}}^{\mathrm{NGR}} = -0.2$, confirming that we have no evidence for a stochastic background alternative gravitational-wave polarizations.

C. Joint fit for GWB and magnetic noise

We extend the standard analysis to do a joint fit allowing for both a GWB with an arbitrary power-law index, as well as an apparent GWB arising from correlated magnetic noise. While we have already seen that correlated magnetic noise is below the O3 sensitivity in Sec. III D, the analysis presented here is complementary because it allows us to simultaneously fit for the presence of both a GWB of astrophysical origin and a correlated magnetic noise component. In future runs, this kind of joint fit will become increasingly important. We use the method described in [62].

We evaluate whether correlated magnetic noise is detected by first constructing a likelihood function that includes a model for both the correlated magnetic noise and a power-law GWB, $\Omega_{\mathrm{M}}(f|\Theta) = \Omega_{\mathrm{PL}}(f|\Theta_{\mathrm{PL}}) + \Omega_{\mathrm{MAG}}(f|\Theta_{\mathrm{MAG}})$. Our model $\Omega_{\mathrm{MAG}}(f|\Theta_{\mathrm{MAG}})$ takes the same form as Eq. (11). However, rather than use the coupling functions measured using magnetic-field injections, we model the coupling functions as power laws, which approximate the frequency dependence of the measurements. The vector Θ_{MAG} contains the parameters of the model for the coupling functions $T_{I,J}(f)$, which we take to be a simple power law

$$|T_I(f)| = \kappa_I \left(\frac{f}{10\ \mathrm{Hz}}\right)^{-\beta_I}. \quad (12)$$

The parameters for the power law GWB are the strength Ω_{ref} and spectral index α. We use nested sampling to estimate the model evidences for three separate models: N, MAG, and PL + MAG, using the notation defined in Sec. II C.

Our prior distribution for the magnitude κ_I is log uniform from 10^{-25} to 10^{-22} pT^{-1} for all of the detectors. Our prior on the spectral index β_I is uniform from β_I^{min} to β_I^{max}, the minimum and maximum values of the spectral index for the magnetic coupling measured at detector I during the O3 run. For Hanford, Livingston and Virgo, the β priors chosen for the study are (0, 12), (1, 10) and (0, 7), respectively. The chosen prior range is large enough to encompass all measured coupling function measurements in O3, including the uncertainties mentioned in Sec. III. We find $\log_{10}\mathcal{B}_{\mathrm{N}}^{\mathrm{MAG}} = -0.03$, which indicates that there is no preference for a model with correlated magnetic noise

TABLE III. Upper limits at the 95% credible level on Ω_{ref} for scalar, vector, and tensor polarizations, along with the improvement of the O3 result over the previous result from O2. We use the log-uniform prior for Ω_{ref} and a Gaussian prior on the spectral index for each polarization, as described in the main text.

Polarization	O3	O2 [44]	Improvement
Tensor	6.4×10^{-9}	3.2×10^{-8}	5.0
Vector	7.9×10^{-9}	2.9×10^{-8}	3.7
Scalar	2.1×10^{-8}	6.1×10^{-8}	2.9

compared to a model with only uncorrelated Gaussian noise. We also consider a model with a power-law GWB present, using the log-uniform prior on Ω_{ref} and Gaussian prior on α as in Sec. IV A. We find that the Bayes factor between a model with correlated GWB and magnetic noise, to a model with only uncorrelated Gaussian noise, is $\log_{10} \mathcal{B}_N^{\text{MAG+PL}} = -0.3$, confirming that there is no evidence of a GWB in the data.

V. IMPLICATIONS FOR COMPACT BINARIES

With upper limits on the GWB in hand, we now explore the implications of these results for the GWB due to CBCs. We first compare our upper limits to updated predictions for the energy-density due to CBC sources. We then combine our limits with the direct detections of CBCs in the local Universe to constrain the merger rate of compact binaries at large redshifts.

A. Fiducial model

Observations from O3a have significantly increased our knowledge of the compact binary population [68,69,71–73,76]. Here, we update the fiducial model of the GWB due to compact binaries [44,63,64,96] in accordance with the latest observational and theoretical advances. The energy-density spectrum due to a particular source class k is

$$\Omega_k(f) = \frac{f}{\rho_c} \int_0^{z_{\text{max}}} dz \frac{R_k(z)\langle (dE_s/df_s)|_{f_s} \rangle_k}{(1+z)H(z)}, \quad (13)$$

where $R_k(z)$ is the source-frame merger rate per comoving volume of objects of class k and $H(z) = H_0\sqrt{\Omega_m(1+z)^3 + \Omega_\Lambda}$ is the Hubble parameter, where Ω_m is the fraction of the critical energy density ρ_c contained in matter and Ω_Λ the fraction contained in the cosmological constant; we take $\Omega_m = 1 - \Omega_\Lambda = 0.3065$ [77]. The quantity $\langle \frac{dE_s}{df_s}|_{f_s} \rangle_k$ is the source-frame energy radiated by a single source, evaluated at the source frequency $f_s = f(1+z)$ and averaged over the ensemble properties of the given class k:

$$\left\langle \frac{dE_s}{df_s} \right\rangle_k = \int d\phi \, p_k(\phi) \frac{dE_s}{df_s}(\phi), \quad (14)$$

where $p_k(\phi)$ is the probability distribution of source parameters ϕ (e.g., masses, spins, etc.) across class k.

We consider here three classes of compact binaries: binary black holes (BBHs), binary neutron stars (BNSs), and neutron-star–black-holes (NSBHs). Except where otherwise stated, we use the same choices for dE_s/df_s, $p_k(\phi)$, and $R_k(z)$ as in [44]. We note that there are several important astrophysical uncertainties which are not included in our fiducial model, which could potentially have an impact on our predictions. These include the

possibility that the initial mass function can lead to a lower number of neutron stars than what we assume [112]; indications that the star formation rate may peak at a smaller redshift [113]; and uncertainty in the metallicity evolution.

1. Binary black holes.

We assume that BBH formation follows a metallicity-weighted star formation rate (SFR) with a distribution $p(t_d) \sim t_d^{-1}$ of time delays t_d between binary formation and merger, where 50 Myr $\leq t_d \leq$ 13.5 Gyr. We take the SFR from Ref. [114], and multiply it by the fraction of stellar formation occurring at metallicities $Z < Z_{\text{thresh}}$ [115]. In Ref. [44], we adopted $Z_{\text{thresh}} = 0.5 \, Z_\odot$, and applied this threshold only to black holes above 30 $M_\odot$. Here, we adopt a more stringent cutoff $Z_{\text{thresh}} = 0.1 \, Z_\odot$ [116,117]. Moreover, we apply this weighting across the entire mass spectrum, as recent population synthesis studies suggest that the mass spectrum of BH mergers does not evolve appreciably with redshift [117].

We additionally update our assumptions regarding the mass and spin distributions of BBHs. In Ref. [44], we assumed that BBHs had aligned dimensionless spin magnitudes distributed uniformly between -1 to 1. It now appears, though, that the BBH population exhibits small effective spins [76,118], and so when computing $\Omega_{\text{BBH}}(f)$ we now assume that BBHs have negligibly small spin. We also adopt a close variant of the *broken power law* model of Ref. [76] to describe the mass distribution of BBHs (for convenience we assume a sharp low-mass cutoff in the BBH mass spectrum, corresponding to $\delta_m \to 0$ in Eq. (B6) of [76]). We do not assume fixed values for the parameters of this model, but include our uncertainty on the BBH mass spectrum as an additional systematic uncertainty in our estimate of $\Omega_{\text{BBH}}(f)$. To achieve this, we use GWTC-2 [68] to hierarchically compute a joint posterior on the mass distribution and local merger rate of BBHs, given the assumed redshift distribution described above. Hierarchical inference is performed following the method discussed in Ref. [76]. By evaluating Eq. (13) across the resulting ensemble of posterior samples, we subsequently obtain a probability distribution on the energy-density spectrum $\Omega_{\text{BBH}}(f)$ due to BBH mergers, given our knowledge of the local population.

Our updated estimate of $\Omega_{\text{BBH}}(f)$ is shown in green in Fig. 5. We find $\Omega_{\text{BBH}}(25 \text{ Hz}) = 4.7^{+1.6}_{-1.4} \times 10^{-10}$. This uncertainty includes the standard Poisson uncertainty on the local merger rate, which we find to be $R_{\text{BBH}}(0) = 19^{+18}_{-8} \text{ Gpc}^{-3} \text{ yr}^{-1}$ (median and symmetric 90% credible interval) given our fiducial redshift distribution above. This rate estimate matches that obtained in Ref. [76] when agnostically allowing the merger rate to evolve with redshift, although in general estimates of $R_{\text{BBH}}(0)$ may differ under different presumed redshift distributions. Our
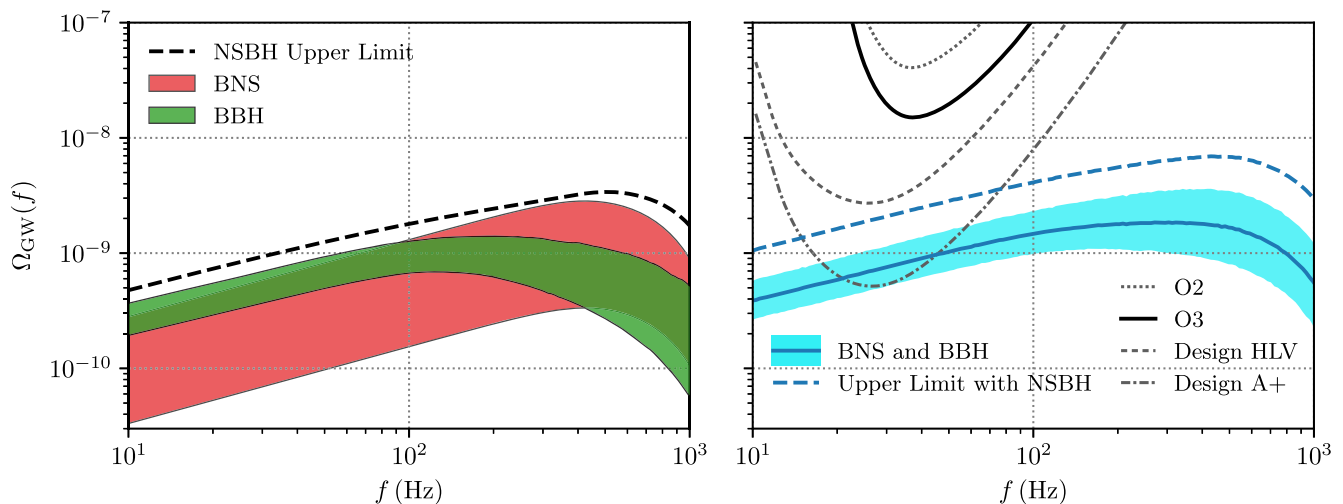
FIG. 5. Fiducial model predictions for the GWB from BBHs, BNSs, and NSBHs, along with current and projected sensitivity curves. In the left panel we show 90% credible bands for the GWB contributions from BNS and BBH mergers. Whereas the BNS uncertainty band illustrates purely the statistical uncertainties in the BNS merger rate, the BBH uncertainty band additionally includes systematic uncertainties in the binary mass distribution, as described in the main text. As no unambiguous NSBH detections have been made, we only show an upper limit on the possible contribution from such systems. The right panel compares the combined BBH and BNS energy density spectra, and 2σ power-law integrated (PI) curves for O2, O3, and projections for the HLV network at design sensitivity, and the A + detectors. The solid blue line shows the median estimate of $\Omega_{\mathrm{BBH+BNS}}(f)$ as a function of frequency, while the shaded blue band illustrates 90% credible uncertainties. The dashed line, meanwhile, marks our projected upper limit on the total GWB, including our upper limit on the contribution from NSBH mergers.

estimate of $\Omega_{\mathrm{BBH}}(25 \text{ Hz})$ also reflects, though, the additional *systematic* uncertainty on $\Omega_{\mathrm{BBH}}(f)$ due to imperfect knowledge of the BBH mass distribution. This uncertainty on the mass distribution is, for example, responsible for the larger uncertainty in $\Omega_{\mathrm{BBH}}(f)$ at high frequencies.

2. Binary neutron stars.

As in [44], we assume that the rate of BNS progenitor formation is proportional to the rate of star formation [114] and that the distribution of time delays t_d between their formation and merger is of the form $p(t_d) \propto t_d^{-1}$ between 20 Myr $\leq t_d \leq 13.5$ Gyr. The detection of a second binary neutron star merger in O3a, GW190425 [70], has decreased uncertainty on the BNS merger rate and demonstrated that at least some neutron star mergers contain significantly heavier masses than expected. Following [76], we assume a uniform distribution of component masses between 1–2.5 $M_\odot$, which yields an estimated present-day merger rate of $R_{\mathrm{BNS}}(0) = 320^{+490}_{-240}$ Gpc^{-3} yr^{-1}. When modeling $\Omega_{\mathrm{BNS}}(f)$, we consider the energy radiated during the inspiral phase only, truncating the BNS energy spectra $\frac{dE_s}{df_s}(\phi)$ at frequencies corresponding to the innermost stable circular orbit. Our estimate of the BNS GWB is shown in red in Fig. 5. We find $\Omega_{\mathrm{BNS}}(25 \text{ Hz}) = 2.0^{+3.2}_{-1.4} \times 10^{-10}$.

3. Neutron star-black hole binaries.

To date, Advanced LIGO and Virgo have made no confirmed detections of neutron star-black hole (NSBH)

mergers. Two events, GW190814 and the low-significance candidate GW190426_152155, have secondary masses constrained below $3\,M_\odot$ with primary masses above $3\,M_\odot$ and so are possibly *consistent* with NSBH systems, but their true physical natures remain unknown [68,73]. In order to forecast the possible contribution of NSBH mergers to the GWB, we therefore use the upper limit on the NSBH merger rate previously adopted in Ref. [44], again assuming a delta-function mass distribution at 10 $M_\odot$ + 1.4 $M_\odot$. We estimate $\Omega_{\mathrm{NSBH}}(f)$ using the same redshift distribution as adopted for BBH mergers, and include contributions from the complete inspiral, merger, and ringdown. This likely results in an *overestimate* of $\Omega_{\mathrm{NSBH}}(f)$ at high frequencies, since some fraction of NSBH inspirals are expected to end in tidal disruption of the neutron star companion [119–121]. The resulting upper limit on $\Omega_{\mathrm{NSBH}}(f)$ is shown as a dashed black line in Fig. 5, with $\Omega_{\mathrm{NSBH}}(25 \text{ Hz}) \leq 8.4 \times 10^{-10}$.

4. Total CBC GWB.

In the right-hand side of Fig. 5 we present an updated estimate of the combined GWB due to BBH and BNS mergers. Under our model, we predict this combined background to be $\Omega_{\mathrm{BBH+BNS}}(25 \text{ Hz}) = 6.8^{+3.6}_{-2.2} \times 10^{-10}$. Combining the upper limit on $\Omega_{\mathrm{NSBH}}(f)$ with the upper 95% credible bound on the contributions from BBH and BNS mergers, we bound the total expected GWB to be $\Omega_{\mathrm{Total}}(25 \text{ Hz}) \leq 1.9 \times 10^{-9}$. We also show the 2σ power-law integrated (PI) curves [99] indicating the integrated sensitivity of the O3 search [99], along with projections for

2 years of the Advanced LIGO-Virgo network at design sensitivity, and the envisioned A + design sensitivity after 2 years, assuming a 50% duty cycle. We use the power spectra available from [122,123]. Previous work has shown that the residual background obtained after subtracting resolvable signals is expected to be within 10% of the total background for Advanced LIGO and Virgo at design sensitivity, and approximately a factor of 2 smaller for the A + detectors [63,106]. These curves indicate that by the time the detectors reach the A + design sensitivity, much of the expected parameter space of the compact binary GWB will be accessible by ground-based detectors. The continued addition of new instruments to the worldwide detector network, like KAGRA [124] and LIGO-India [125], is expected to further improve upon our projected sensitivity. For coincident and co-aligned detectors with the same power spectral density, the improvement in sensitivity should scale like the square root of the number of baselines, or equivalently with the number of detectors in the network. However, in practice one must account for the different overlap reduction functions for each baseline, as well as for different sensitivities. Reference [99] gives a prescription for a general set of detectors. Figure 9 of that paper indicates that the improvement is likely to be minimal for small power laws, and becomes larger for large power laws.

B. Constraining the BBH merger rate

The energy-density spectra in Fig. 5 show our current best estimates for the GWB under an astrophysically plausible model for the rate density $R_{\mathrm{BBH}}(z)$ of BBH mergers of stellar origin. By combining direct detections of compact binaries with upper limits on the GWB, however, we can alternatively seek to directly measure $R_{\mathrm{BBH}}(z)$. Knowledge of the BBH redshift distribution, and in particular the redshift at which $R_{\mathrm{BBH}}(z)$ is at a maximum, offers a potential measure of the mean evolutionary time delay between binary formation and merger, the branching ratios between competing formation channels, or even the underlying star formation rate [126,127]. Although the measurement of $R_{\mathrm{BBH}}(z)$ is made difficult by the limited range of present ground-based detectors, we can nevertheless make progress by combining direct BBH detections with upper limits on the GWB [75].

Here, we update the constraints on the rate evolution of BBHs from [75], using our latest O3 limits on the GWB and the expanded GWTC-2 catalog of BBH detections. We again assume a *broken power law* form for the mass distribution of BBH mergers, but now adopt a phenomenologically-parametrized form

$$R_{\mathrm{BBH}}(z) = \mathcal{C}(\lambda_1, \lambda_2, z_{\mathrm{peak}}) \frac{R_0(1+z)^{\lambda_1}}{1 + (\frac{1+z}{1+z_{\mathrm{peak}}})^{\lambda_1+\lambda_2}} \quad (15)$$

for their merger rate density. Under this form, the merger rate evolves as $R_{\mathrm{BBH}}(z) \approx (1+z)^{\lambda_1}$ at $z \lesssim z_{\mathrm{peak}}$ and $R_{\mathrm{BBH}} \approx (1+z)^{-\lambda_2}$ at $z \gtrsim z_{\mathrm{peak}}$, and at low redshifts λ_1 can be
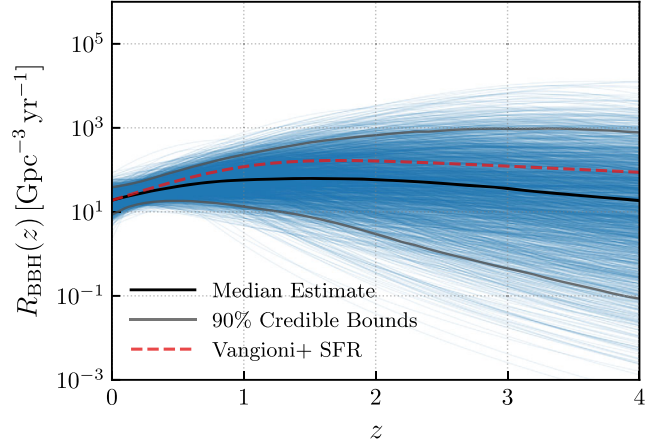

FIG. 6. Posterior constraints on the BBH merger rate $R_{\mathrm{BBH}}(z)$ as a function of redshift when allowing for a merger rate that peaks and subsequently turns over at high z, combining stochastic search results and direct BBH detections. The black line shows our median estimate of $R_{\mathrm{BBH}}(z)$, while solid grey lines denote 90% credible bounds. For comparison, the dashed red line is proportional to the rate of cosmic star formation [114]. At 90% credibility, the merger rate of BBHs is bounded below $\sim 10^3$ Gpc^{-3} yr^{-1} beyond $z \approx 2$, an order of magnitude improvement relative to O1 and O2 [75].

identified with the parameter κ of Ref. [76]. The normalization constant $\mathcal{C}(\lambda_1, \lambda_2, z_{\mathrm{peak}})$ is defined such that R_0 is the local merger rate density of BBHs at $z = 0$.

Using the direct BBH detections from GWTC-2 along with the updated GWB search results presented here, we jointly infer the parameters governing both the mass and redshift distributions of BBH mergers. We adopt the factorized likelihood from Eq. (9), given by the product between the standard GWB likelihood $p(C^{IJ}(f_k)|\Theta_{\mathrm{BBH}})$ under our model for the BBH background, and the likelihood $p(\{d\}|\Theta_{\mathrm{BBH}})$ of having measured data $\{d\}$ associated with the 44 direct BBH detections in GWTC-2 with false alarm rates < 1 yr^{-1}. This likelihood $p(\{d\}|\Theta_{\mathrm{BBH}})$ for direct detections is evaluated using posterior samples on the parameters of each individual event, as described further in Sec. 4 of [76]. The direct detection likelihood also corrects for selection biases, such as LIGO and Virgo's higher detection efficiency for higher-mass systems; we evaluate selection effects using the same injection campaign discussed in [76]. Our priors are uniform on λ_1, λ_2, and z_{peak}, and log-uniform on R_0.

The resulting constraints on the BBH merger rate as a function of redshift are shown in Fig. 6. Each blue trace represents a single draw from our posterior on the BBH mass distribution and merger rate history. The black curve marks the median estimated merger rate at a given redshift, while solid grey curves mark our central 90% credible bound. From O1 and O2 data, the nondetection of the GWB served to constrain the BBH merger rate to less than $\sim 10^4$ Gpc^{-3} yr^{-1} beyond $z \approx 2$ at 90% credibility [75].
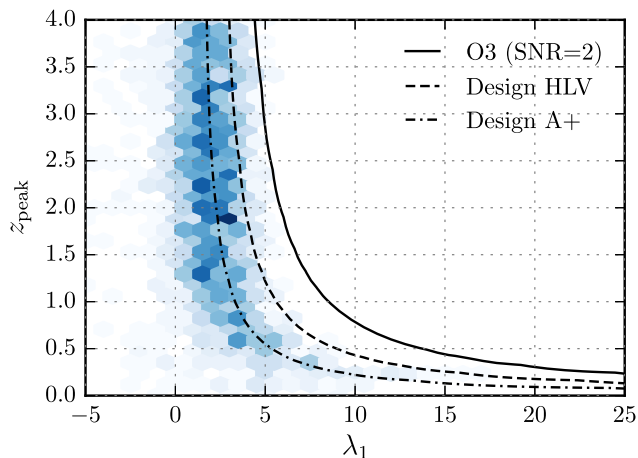
FIG. 7. 2D posterior density for joint CBC-GWB inference on the parameters λ_1 and z_{peak} describing the BBH redshift distribution, defined in the main text. While the O3 stochastic measurement (solid line) is not competitive with measurements on z_{peak} and λ_1 obtained from GWTC-2 (shown as a blue posterior density), stochastic background measurements from future observing runs (dashed lines) may be able to put tighter constraints on these parameters in combinations with observations of individual binaries.

This limit is here improved by a factor of approximately ten. For reference, the dashed red curve is proportional to the star formation rate model of Ref. [114]. While the BBH merger rate remains consistent with directly tracing star formation, it likely increases more slowly as a function of redshift, consistent with a nonvanishing time delay distribution between binary formation and merger [76].

While O1/O2 constraints on the behavior of $R_{BBH}(z)$ at redshifts $z \gtrsim 0.5$ were dominated by stochastic search results [75], the results in Fig. 6 from O3 are now due primarily to the direct detections comprising GWTC-2. The cause for this shift is illustrated in Fig. 7, which shows our joint $\lambda_1 - z_{peak}$ posterior (informed by both GWB data and direct BBH detections), marginalized over the remaining parameters governing the BBH mass and redshift distributions. The solid black contour show the values of λ_1 and z_{peak} expected to yield a GWB detection with SNR = 2 in O3; values to the right of this contour can be excluded on the basis of a GWB nondetection. Direct BBH detections, meanwhile, allow for a measurement of λ_1, but are not expected to meaningfully constrain z_{peak}, which likely lies beyond the horizon of Advanced LIGO and Virgo. The direct BBH detections in GWTC-1 only allowed for a weak upper limit on λ_1: $\lambda_1 \leq 13.7$. The nondetection of the GWB in O2 therefore ruled out a considerable portion of otherwise available parameter space. Improved measurements due to GWTC-2, though, have revised estimates of λ_1 downwards to $\lambda_1 = 1.3^{+2.1}_{-2.1}$ [76], and so present GWB searches cannot further constrain its value. The results in Fig. 6 are therefore now dominated by direct BBH detections.

With continued data collection, however, the nondetection (or eventual detection) of the GWB may again offer informative constraints on λ_1 and z_{peak}. As additional direct BBH detections are made, our knowledge of λ_1 will continue to improve, identifying an increasingly narrow, nearly-vertical contour in the $\lambda_1 - z_{peak}$ plane. Continued time integration in searches for the GWB, meanwhile, will exclude a growing fraction of this plane, ruling out large values of *both* λ_1 and z_{peak}. In Fig. 7, for example, we show projected exclusion contours corresponding to one year of integration with Advanced LIGO and Virgo, at both their design sensitivity and A + configurations; both exclusion curves extend into the presently allowed values of λ_1, where they may again be informative and break the degeneracy between λ_1 and z_{peak}.

VI. CONCLUSIONS

In this work, we have performed a search for an isotropic GWB using data from Advanced LIGO's and Virgo's first three observing runs. Since we did not find evidence for a background of astrophysical origin, we placed upper limits, improving previous bounds by about a factor of 6.0 for a flat background.

We considered the implications of the results, and by combining the upper limits with measurements from GWTC-2 we have constrained the BBH merger rate as a function of redshift. Our results can be used to constrain additional models such as cosmic strings [128] or phase transitions [129], using the cross correlation spectra we have made publicly available [58]. Our results can also be combined with other measurements of the GWB at other frequencies [82]. Although in this work we focused on searching for an isotropic GWB, in a companion paper we present a search for an anisotropic GWB using data from LIGO and Virgo's third observing run [130].

Moving forward, we expect currently proposed ground-based facilities such as A+ have the potential to probe a large range of the model space for CBC backgrounds. In order to make full use of the data and confidently claim a detection, it will be important to further develop the methods to handle correlated terrestrial noise sources, such as the magnetic couplings described here.

[1] N. J. Cornish and J. D. Romano, Phys. Rev. D **92**, 042001 (2015).

[2] P. A. Rosado, Phys. Rev. D **84**, 084004 (2011).

[3] X.-J. Zhu, E. Howell, T. Regimbau, D. Blair, and Z.-H. Zhu, Astrophys. J. **739**, 86 (2011).

[4] S. Marassi, R. Schneider, G. Corvino, V. Ferrari, and S. P. Zwart, Phys. Rev. D **84**, 124037 (2011).

[5] C. Wu, V. Mandic, and T. Regimbau, Phys. Rev. D **85**, 104024 (2012).

[6] X.-J. Zhu, E. J. Howell, D. G. Blair, and Z.-H. Zhu, Mon. Not. R. Astron. Soc. **431**, 882 (2013).

[7] A. Buonanno, G. Sigl, G. G. Raffelt, H.-T. Janka, and E. Muller, Phys. Rev. D **72**, 084001 (2005).

[8] E. Howell, D. Coward, R. Burman, D. Blair, and J. Gilmore, Mon. Not. R. Astron. Soc. **351**, 1237 (2004).

[9] P. Sandick, K. A. Olive, F. Daigne, and E. Vangioni, Phys. Rev. D **73**, 104024 (2006).

[10] S. Marassi, R. Schneider, and V. Ferrari, Mon. Not. R. Astron. Soc. **398**, 293 (2009).

[11] X.-J. Zhu, E. Howell, and D. Blair, Mon. Not. R. Astron. Soc. **409**, L132 (2010).

[12] V. Ferrari, S. Matarrese, and R. Schneider, Mon. Not. R. Astron. Soc. **303**, 258 (1999).

[13] T. Regimbau and J. A. de Freitas Pacheco, Astron. Astrophys. **376**, 381 (2001).

[14] E. Howell, T. Regimbau, A. Corsi, D. Coward, and R. Burman, Mon. Not. R. Astron. Soc. **410**, 2123 (2011).

[15] X.-J. Zhu, X.-L. Fan, and Z.-H. Zhu, Astrophys. J. **729**, 59 (2011).

[16] S. Marassi, R. Ciolfi, R. Schneider, L. Stella, and V. Ferrari, Mon. Not. R. Astron. Soc. **411**, 2549 (2011).

[17] P. A. Rosado, Phys. Rev. D **86**, 104007 (2012).

[18] C.-J. Wu, V. Mandic, and T. Regimbau, Phys. Rev. D **87**, 042002 (2013).

[19] P. D. Lasky, M. F. Bennett, and A. Melatos, Phys. Rev. D **87,** 063004 (2013).
[20] K. Crocker, V. Mandic, T. Regimbau, K. Belczynski, W. Gladysz, K. Olive, T. Prestegard, and E. Vangioni, Phys. Rev. D **92,** 063005 (2015).
[21] K. Crocker, T. Prestegard, V. Mandic, T. Regimbau, K. Olive, and E. Vangioni, Phys. Rev. D **95,** 063015 (2017).
[22] T. W. B. Kibble, J. Phys. A **9,** 1387 (1976).
[23] S. Sarangi and S.-H. H. Tye, Phys. Lett. B **536,** 185 (2002).
[24] T. Damour and A. Vilenkin, Phys. Rev. D **71,** 063510 (2005).
[25] X. Siemens, V. Mandic, and J. Creighton, Phys. Rev. Lett. **98,** 111101 (2007).
[26] B. Abbott *et al.* (LIGO Scientific and Virgo Collaborations), Phys. Rev. D **97,** 102002 (2018).
[27] M. Sasaki, T. Suyama, T. Tanaka, and S. Yokoyama, Phys. Rev. Lett. **117,** 061101 (2016).
[28] V. Mandic, S. Bird, and I. Cholis, Phys. Rev. Lett. **117,** 201102 (2016).
[29] S. Wang, Y.-F. Wang, Q.-G. Huang, and T. G. F. Li, Phys. Rev. Lett. **120,** 191102 (2018).
[30] R. Brito, S. Ghosh, E. Barausse, E. Berti, V. Cardoso, I. Dvorkin, A. Klein, and P. Pani, Phys. Rev. Lett. **119,** 131101 (2017).
[31] R. Brito, S. Ghosh, E. Barausse, E. Berti, V. Cardoso, I. Dvorkin, A. Klein, and P. Pani, Phys. Rev. D **96,** 064050 (2017).
[32] X.-L. Fan and Y.-B. Chen, Phys. Rev. D **98,** 044020 (2018).
[33] L. Tsukada, T. Callister, A. Matas, and P. Meyers, Phys. Rev. D **99,** 103015 (2019).
[34] A. Lopez and K. Freese, J. Cosmol. Astropart. Phys. 01 (2015) 037.
[35] P. S. B. Dev and A. Mazumdar, Phys. Rev. D **93,** 104001 (2016).
[36] L. Marzola, A. Racioppi, and V. Vaskonen, Eur. Phys. J. C **77,** 484 (2017).
[37] B. Von Harling, A. Pomarol, O. Pujolas, and F. Rompineve, J. High Energy Phys. 04 (2020) 195.
[38] C. Caprini and D. G. Figueroa, Classical Quantum Gravity **35,** 163001 (2018).
[39] A. A. Starobinskiĭ, JETP Lett. **30,** 682 (1979), https://ui.adsabs.harvard.edu/abs/1979JETPL..30..682S/abstract.
[40] M. S. Turner, Phys. Rev. D **55,** R435 (1997).
[41] R. Bar-Kana, Phys. Rev. D **50,** 1157 (1994).
[42] R. Easther and E. A. Lim, J. Cosmol. Astropart. Phys. 4 (2006) 010.
[43] R. Easther, J. T. Giblin, Jr., and E. A. Lim, Phys. Rev. Lett. **99,** 221301 (2007).
[44] B. Abbott *et al.* (LIGO Scientific and Virgo Collaborations), Phys. Rev. D **100,** 061101 (2019).
[45] B. Abbott *et al.* (LIGO Scientific and Virgo Collaborations), Phys. Rev. D **100,** 062001 (2019).
[46] T. Callister, A. S. Biscoveanu, N. Christensen, M. Isi, A. Matas, O. Minazzoli, T. Regimbau, M. Sakellariadou, J. Tasson, and E. Thrane, Phys. Rev. X **7,** 041058 (2017).
[47] B. P. Abbott *et al.* (LIGO Scientific and Virgo Collaborations), Phys. Rev. Lett. **120,** 201102 (2018).
[48] J. D. Romano and N. J. Cornish, Living Rev. Relativity **20,** 2 (2017).
[49] N. Christensen, Rep. Prog. Phys. **82,** 016903 (2019).
[50] R. Abbott *et al.* (LIGO Scientific and Virgo Collaborations), SoftwareX **13,** 100658 (2021).
[51] A. Renzini and C. Contaldi, Mon. Not. R. Astron. Soc. **481,** 4650 (2018).
[52] A. I. Renzini and C. R. Contaldi, Phys. Rev. Lett. **122,** 081102 (2019).
[53] A. Renzini and C. Contaldi, Phys. Rev. D **100,** 063527 (2019).
[54] R. Smith and E. Thrane, Phys. Rev. X **8,** 021019 (2018).
[55] J. Aasi *et al.* (LIGO Scientific Collaboration), Classical Quantum Gravity **32,** 074001 (2015).
[56] F. Acernese *et al.*, Classical Quantum Gravity **32,** 024001 (2015).
[57] H. Jeffreys, Proc. R. Soc. A **186,** 453 (1946).
[58] R. Abbott *et al.* (LIGO Scientific and Virgo Collaborations), https://dcc.ligo.org/G2001287/public.
[59] B. Allen and J. D. Romano, Phys. Rev. D **59,** 102001 (1999).
[60] K. Riles and J. Zweizig, https://dcc.ligo.org/T2000384/public (2021).
[61] A. Matas, I. Dvorkin, T. Regimbau, and A. Romero, https://dcc.ligo.org/P2000546/public (2021).
[62] P. M. Meyers, K. Martinovic, N. Christensen, and M. Sakellariadou, Phys. Rev. D **102,** 102005 (2020).
[63] B. P. Abbott *et al.* (LIGO Scientific and Virgo Collaborations), Phys. Rev. Lett. **116,** 131102 (2016).
[64] B. P. Abbott *et al.* (LIGO Scientific and Virgo Collaborations), Phys. Rev. Lett. **120,** 091101 (2018).
[65] T. Regimbau *et al.*, Phys. Rev. D **86,** 122001 (2012).
[66] T. Regimbau, D. Meacher, and M. Coughlin, Phys. Rev. D **89,** 084046 (2014).
[67] D. Meacher, M. Coughlin, S. Morris, T. Regimbau, N. Christensen, S. Kandhasamy, V. Mandic, J. D. Romano, and E. Thrane, Phys. Rev. D **92,** 063002 (2015).
[68] R. Abbott *et al.* (LIGO Scientific and Virgo Collaborations), Phys. Rev. X **11,** 021053 (2011).
[69] R. Abbott *et al.* (LIGO Scientific and Virgo Collaborations), Phys. Rev. D **102,** 043015 (2020).
[70] B. Abbott *et al.* (LIGO Scientific and Virgo Collaborations), Astrophys. J. Lett. **892,** L3 (2020).
[71] R. Abbott *et al.* (LIGO Scientific and Virgo Collaborations), Phys. Rev. Lett. **125,** 101102 (2020).
[72] R. Abbott *et al.* (LIGO Scientific and Virgo Collaborations), Astrophys. J. Lett. **900,** L13 (2020).
[73] R. Abbott *et al.* (LIGO Scientific and Virgo Collaborations), Astrophys. J. **896,** L44 (2020).
[74] L. Barsotti, L. McCuller, M. Evans, and P. Fritschel, https://dcc.ligo.org/LIGO-T1800042/public ().
[75] T. Callister, M. Fishbach, D. Holz, and W. Farr, Astrophys. J. **896,** L32 (2020).
[76] R. Abbott *et al.* (LIGO Scientific and Virgo Collaborations), Astrophys. J. Lett. **913,** L7 (2021).
[77] P. A. R. Ade *et al.*, Astron. Astrophys. **594,** A13 (2016).
[78] N. Christensen, Phys. Rev. D **46,** 5250 (1992).
[79] C. M. F. Mingarelli, S. R. Taylor, B. S. Sathyaprakash, and W. M. Farr, arXiv:1911.09745.
[80] V. Mandic, E. Thrane, S. Giampanis, and T. Regimbau, Phys. Rev. Lett. **109,** 171102 (2012).
[81] A. Matas and J. D. Romano, Phys. Rev. D **103,** 062003 (2021).
[82] P. D. Lasky *et al.*, Phys. Rev. X **6,** 011035 (2016).

[83] http://www.lemisensors.com.

[84] https://www.geo-metronix.de/mtxgeo/index.php/mfs-06e-overview.

[85] https://git.ligo.org/stochastic-public/stochastic/.

[86] MATLAB, 9.8.0.1323502 (R2020a) (The MathWorks Inc., Natick, Massachusetts, 2020).

[87] C. Biwer *et al.*, Phys. Rev. D **95**, 062002 (2017).

[88] B. P. Abbott *et al.* (LIGO Scientific and Virgo Collaborations), Classical Quantum Gravity **35**, 065010 (2018).

[89] D. Davis *et al.*, arXiv:2101.11673.

[90] P. Covas *et al.* (LSC Instrument Authors), Phys. Rev. D **97**, 082002 (2018).

[91] P. Nguyen *et al.* , Environmental noise in Advanced LIGO detectors, Classical Quantum Gravity **38**, 145001 (2021).

[92] W. Schumann, Z. Naturforsch. **7A**, 250 (1952).

[93] M. W. Coughlin *et al.*, Phys. Rev. D **97**, 102007 (2018).

[94] E. Thrane, N. Christensen, and R. Schofield, Phys. Rev. D **87**, 123009 (2013).

[95] E. Thrane, N. Christensen, R. M. S. Schofield, and A. Effler, Phys. Rev. D **90**, 023013 (2014).

[96] B. P. Abbott *et al.* (LIGO Scientific and Virgo Collaborations), Phys. Rev. Lett. **118**, 121101 (2017).

[97] K. Merfeld *et al.*, aLIGO LHO Logbook, https://alog.ligo-wa.caltech.edu/aLOG/index.php?callRep=48212.

[98] P. Nguyen *et al.*, aLIGO LHO Logbook, https://alog.ligo-wa.caltech.edu/aLOG/index.php?callRep=57672 ().

[99] E. Thrane and J. D. Romano, Phys. Rev. D **88**, 124032 (2013).

[100] P. Nguyen *et al.*, aLIGO LHO Logbook, https://alog.ligo-wa.caltech.edu/aLOG/index.php?callRep=43406 ().

[101] I. Michaloliakos *et al.*, aLIGO LHO Logbook, https://alog.ligo-wa.caltech.edu/aLOG/index.php?callRep=56295.

[102] T. Regimbau, Res. Astron. Astrophys. **11**, 369 (2011).

[103] C. Périgois, C. Belczynski, T. Bulik, and T. Regimbau, Phys. Rev. D **103**, 043002 (2021).

[104] J. M. Ezquiaga and D. E. Holz, Astrophys. J. Lett. **909**, L23 (2021).

[105] P. Sandick, K. A. Olive, F. Daigne, and E. Vangioni, Phys. Rev. D **73**, 104024 (2006).

[106] T. Regimbau, M. Evans, N. Christensen, E. Katsavounidis, B. Sathyaprakash, and S. Vitale, Phys. Rev. Lett. **118**, 151105 (2017).

[107] S. Sachdev, T. Regimbau, and B. Sathyaprakash, Phys. Rev. D **102**, 024051 (2020).

[108] K. Martinovic, P. M. Meyers, M. Sakellariadou, and N. Christensen, Phys. Rev. D **103**, 043023 (2021).

[109] J. T. Whelan, E. L. Robinson, J. D. Romano, and E. H. Thrane, J. Phys. Conf. Ser. **484**, 012027 (2014).

[110] L. Sun *et al.*, Classical Quantum Gravity **37**, 225008 (2020).

[111] M. Isi and L. C. Stein, Phys. Rev. D **98**, 104025 (2018).

[112] M. Chrúslínská, T. Jerábková, G. Nelemans, and Z. Yan, Astron. Astrophys. **636**, A10 (2020).

[113] R. López Fernández, R. M. González Delgado, E. Pérez, R. García-Benito, R. Cid Fernandes, W. Schoenell, S. F. Sánchez, A. Gallazzi, P. Sánchez-Blázquez, N. Vale Asari, and C. J. Walcher, Astron. Astrophys. **615**, A27 (2018).

[114] E. Vangioni, K. A. Olive, T. Prestegard, J. Silk, P. Petitjean, and V. Mandic, Mon. Not. R. Astron. Soc. **447**, 2575 (2015).

[115] N. Langer and C. A. Norman, Astrophys. J. Lett. **638**, L63 (2006).

[116] M. Chruslinska, G. Nelemans, and K. Belczynski, Mon. Not. R. Astron. Soc. **482**, 5012 (2019).

[117] M. Mapelli, N. Giacobbo, F. Santoliquido, and M. C. Artale, Mon. Not. R. Astron. Soc. **487**, 2 (2019).

[118] S. Miller, T. A. Callister, and W. Farr, Astrophys. J. **895**, 128 (2020).

[119] F. Foucart, M. D. Duez, L. E. Kidder, and S. A. Teukolsky, Phys. Rev. D **83**, 024005 (2011).

[120] K. Kyutoku, M. Shibata, and K. Taniguchi, Phys. Rev. D **82**, 044049 (2010).

[121] K. Kawaguchi, K. Kyutoku, H. Nakano, H. Okawa, M. Shibata, and K. Taniguchi, Phys. Rev. D **92**, 024014 (2015).

[122] B. Abbott *et al.* (KAGRA, LIGO Scientific, and VIRGO Collaborations), Living Rev. Relativity **21**, 3 (2018).

[123] L. Barsotti, P. Fritschel, M. Evans, and S. Gras, https://dcc.ligo.org/T1800044-v5/public ().

[124] T. Akutsu, M. Ando, K. Arai, Y. Arai, S. Araki *et al.*, arXiv:2005.05574.

[125] B. Iyer, T. Souradeep, C. S. Unnikrishnan, S. Dhurandhar, S. Raja, A. Kumar, and A. Sengupta, LIGO-India Technical Report No. LIGO-M1100296, 2011.

[126] S. Vitale, W. M. Farr, K. K. Y. Ng, and C. L. Rodriguez, Astrophys. J. **886**, L1 (2019).

[127] K. K. Y. Ng, S. Vitale, W. M. Farr, and C. L. Rodriguez, Astrophys. J. Lett. **913**, L5 (2021).

[128] R. Abbott *et al.* (LIGO Scientific, Virgo, and KAGRA Collaborations), Phys. Rev. Lett. **126**, 241102 (2021).

[129] R. Romero, K. Martinovic, T. Callister, H.-K. Guo, M. Martínez, M. Sakellariadou, F.-W. Yang, and Y. Zhao, Phys. Rev. Lett. **126**, 151301 (2021).

[130] R. Abbott *et al.* (LIGO Scientific, Virgo, and KAGRA Collaborations), arXiv:2103.08520.

[131] J. D. Hunter, Comput. Sci. Eng. **9**, 90 (2007).

R. Abbott,[1] T. D. Abbott,[2] S. Abraham,[3] F. Acernese,[4,5] K. Ackley,[6] A. Adams,[7] C. Adams,[8] R. X. Adhikari,[1] V. B. Adya,[9] C. Affeldt,[10,11] D. Agarwal,[3] M. Agathos,[12,13] K. Agatsuma,[14] N. Aggarwal,[15] O. D. Aguiar,[16] L. Aiello,[17,18,19] A. Ain,[20,21] T. Akutsu,[22,23] K. M. Aleman,[24] G. Allen,[25] A. Allocca,[26,5] P. A. Altin,[9] A. Amato,[27] S. Anand,[1] A. Ananyeva,[1] S. B. Anderson,[1] W. G. Anderson,[28] M. Ando,[29,30] S. V. Angelova,[31] S. Ansoldi,[32,33] J. M. Antelis,[34] S. Antier,[35] S. Appert,[1] Koya Arai,[36] Koji Arai,[1] Y. Arai,[36] S. Araki,[37] A. Araya,[38] M. C. Araya,[1] J. S. Areeda,[24] M. Arène,[35] N. Aritomi,[29] N. Arnaud,[39,40] S. M. Aronson,[41] H. Asada,[42] Y. Asali,[43] G. Ashton,[6] Y. Aso,[44,45] S. M. Aston,[8] P. Astone,[46] F. Aubin,[47] P. Aufmuth,[10,11] K. AultONeal,[34] C. Austin,[2] S. Babak,[35] F. Badaracco,[18,19] M. K. M. Bader,[48] S. Bae,[49] Y. Bae,[50]

A. M. Baer,[7] S. Bagnasco,[51] Y. Bai,[1] L. Baiotti,[52] J. Baird,[35] R. Bajpai,[53] M. Ball,[54] G. Ballardin,[40] S. W. Ballmer,[55] M. Bals,[34] A. Balsamo,[7] G. Baltus,[56] S. Banagiri,[57] D. Bankar,[3] R. S. Bankar,[3] J. C. Barayoga,[1] C. Barbieri,[58,59,60] B. C. Barish,[1] D. Barker,[61] P. Barneo,[62] S. Barnum,[63] F. Barone,[64,5] B. Barr,[65] L. Barsotti,[63] M. Barsuglia,[35] D. Barta,[66] J. Bartlett,[61] M. A. Barton,[65,22] I. Bartos,[41] R. Bassiri,[67] A. Basti,[21,20] M. Bawaj,[68,69] J. C. Bayley,[65] A. C. Baylor,[28] M. Bazzan,[70,71] B. Bécsy,[72] V. M. Bedakihale,[73] M. Bejger,[74] I. Belahcene,[39] V. Benedetto,[75] D. Beniwal,[76] M. G. Benjamin,[34] T. F. Bennett,[77] J. D. Bentley,[14] M. BenYaala,[31] F. Bergamin,[10,11] B. K. Berger,[67] S. Bernuzzi,[13,15] D. Bersanetti,[78] A. Bertolini,[48] J. Betzwieser,[8] R. Bhandare,[79] A. V. Bhandari,[3] D. Bhattacharjee,[80] S. Bhaumik,[41] J. Bidler,[24] I. A. Bilenko,[81] G. Billingsley,[1] R. Birney,[82] O. Birnholtz,[83] S. Biscans,[1,63] M. Bischi,[84,85] S. Biscoveanu,[63] A. Bisht,[10,11] B. Biswas,[3] M. Bitossi,[40,20] M.-A. Bizouard,[86] J. K. Blackburn,[1] J. Blackman,[87] C. D. Blair,[88,8] D. G. Blair,[88] R. M. Blair,[61] F. Bobba,[89,90] N. Bode,[10,11] M. Boer,[86] G. Bogaert,[86] M. Boldrini,[91,46] F. Bondu,[92] E. Bonilla,[67] R. Bonnand,[47] P. Booker,[10,11] B. A. Boom,[48] R. Bork,[1] V. Boschi,[20] N. Bose,[93] S. Bose,[3] V. Bossilkov,[88] V. Boudart,[56] Y. Bouffanais,[70,71] A. Bozzi,[40] C. Bradaschia,[20] P. R. Brady,[28] A. Bramley,[8] A. Branch,[8] M. Branchesi,[18,19] J. E. Brau,[54] M. Breschi,[13] T. Briant,[94] J. H. Briggs,[65] A. Brillet,[86] M. Brinkmann,[10,11] P. Brockill,[28] A. F. Brooks,[1] J. Brooks,[40] D. D. Brown,[76] S. Brunett,[1] G. Bruno,[95] R. Bruntz,[7] J. Bryant,[14] A. Buikema,[63] T. Bulik,[96] H. J. Bulten,[48,97] A. Buonanno,[98,99] R. Buscicchio,[14] D. Buskulic,[47] R. L. Byer,[67] L. Cadonati,[100] M. Caesar,[101] G. Cagnoli,[27] C. Cahillane,[1] H. W. Cain III,[2] J. Calderón Bustillo,[102] J. D. Callaghan,[65] T. A. Callister,[103,104] E. Calloni,[26,5] J. B. Camp,[105] M. Canepa,[106,78] M. Cannavacciuolo,[89] K. C. Cannon,[30] H. Cao,[76] J. Cao,[107] Z. Cao,[108] E. Capocasa,[22] E. Capote,[24] G. Carapella,[89,90] F. Carbognani,[40] J. B. Carlin,[109] M. F. Carney,[15] M. Carpinelli,[110,111] G. Carullo,[21,20] T. L. Carver,[17] J. Casanueva Diaz,[40] C. Casentini,[112,113] G. Castaldi,[114] S. Caudill,[48,115] M. Cavaglià,[80] F. Cavalier,[39] R. Cavalieri,[40] G. Cella,[20] P. Cerdá-Durán,[116] E. Cesarini,[113] W. Chaibi,[86] K. Chakravarti,[3] B. Champion,[117] C.-H. Chan,[118] C. Chan,[30] C. L. Chan,[102] M. Chan,[119] K. Chandra,[93] P. Chanial,[40] S. Chao,[118] P. Charlton,[120] E. A. Chase,[15] E. Chassande-Mottin,[35] D. Chatterjee,[28] M. Chaturvedi,[79] A. Chen,[102] C. Chen,[121,122] H. Y. Chen,[123] J. Chen,[118] K. Chen,[124] X. Chen,[88] Y.-B. Chen,[87] Y.-R. Chen,[122] Z. Chen,[17] H. Cheng,[41] C. K. Cheong,[102] H. Y. Cheung,[102] H. Y. Chia,[41] F. Chiadini,[125,90] C-Y. Chiang,[126] R. Chierici,[127] A. Chincarini,[78] M. L. Chiofalo,[21,20] A. Chiummo,[40] G. Cho,[128] H. S. Cho,[129] S. Choate,[101] R. K. Choudhary,[88] S. Choudhary,[3] N. Christensen,[86] H. Chu,[124] Q. Chu,[88] Y-K. Chu,[126] S. Chua,[94] K. W. Chung,[130] G. Ciani,[70,71] P. Ciecielag,[74] M. Cieślar,[74] M. Cifaldi,[112,113] A. A. Ciobanu,[76] R. Ciolfi,[131,71] F. Cipriano,[86] A. Cirone,[106,78] F. Clara,[61] E. N. Clark,[132] J. A. Clark,[100] L. Clarke,[133] P. Clearwater,[109] S. Clesse,[134] F. Cleva,[86] E. Coccia,[18,19] P.-F. Cohadon,[94] D. E. Cohen,[39] L. Cohen,[2] M. Colleoni,[135] C. G. Collette,[136] M. Colpi,[58,59] C. M. Compton,[61] M. Constancio Jr.,[16] L. Conti,[71] S. J. Cooper,[14] P. Corban,[8] T. R. Corbitt,[2] I. Cordero-Carrión,[137] S. Corezzi,[69,68] K. R. Corley,[43] N. Cornish,[72] D. Corre,[39] A. Corsi,[138] S. Cortese,[40] C. A. Costa,[16] R. Cotesta,[99] M. W. Coughlin,[57] S. B. Coughlin,[15,17] J.-P. Coulon,[86] S. T. Countryman,[43] B. Cousins,[139] P. Couvares,[1] P. B. Covas,[135] D. M. Coward,[88] M. J. Cowart,[8] D. C. Coyne,[1] R. Coyne,[140] J. D. E. Creighton,[28] T. D. Creighton,[141] A. W. Criswell,[57] T. D. Creighton,[141] A. W. Criswell,[57] M. Croquette,[94] S. G. Crowder,[142] J. R. Cudell,[56] T. J. Cullen,[2] A. Cumming,[65] R. Cummings,[65] E. Cuoco,[40,143,20] M. Curyło,[96] T. Dal Canton,[99,39] G. Dálya,[144] A. Dana,[67] L. M. DaneshgaranBajastani,[77] B. D'Angelo,[106,78] S. L. Danilishin,[145] S. D'Antonio,[113] K. Danzmann,[10,11] C. Darsow-Fromm,[146] A. Dasgupta,[73] L. E. H. Datrier,[65] V. Dattilo,[40] I. Dave,[79] M. Davier,[39] G. S. Davies,[147,148] D. Davis,[1] E. J. Daw,[149] R. Dean,[101] M. Deenadayalan,[3] J. Degallaix,[150] M. De Laurentis,[26,5] S. Déléglise,[94] V. Del Favero,[117] F. De Lillo,[95] N. De Lillo,[65] W. Del Pozzo,[21,20] L. M. DeMarchi,[15] F. De Matteis,[112,113] V. D'Emilio,[17] N. Demos,[63] T. Dent,[147] A. Depasse,[95] R. De Pietri,[151,152] R. De Rosa,[26,5] C. De Rossi,[40] R. DeSalvo,[114] R. De Simone,[125] S. Dhurandhar,[3] M. C. Díaz,[141] M. Diaz-Ortiz Jr.,[41] N. A. Didio,[55] T. Dietrich,[99] L. Di Fiore,[5] C. Di Fronzo,[14] C. Di Giorgio,[89,90] F. Di Giovanni,[116] T. Di Girolamo,[26,5] A. Di Lieto,[21,20] B. Ding,[136] S. Di Pace,[91,46] I. Di Palma,[91,46] F. Di Renzo,[21,20] A. K. Divakarla,[41] A. Dmitriev,[14] Z. Doctor,[54] L. D'Onofrio,[26,5] F. Donovan,[63] K. L. Dooley,[17] S. Doravari,[3] I. Dorrington,[17] M. Drago,[18,19] J. C. Driggers,[61] Y. Drori,[1] Z. Du,[107] J.-G. Ducoin,[39] P. Dupej,[65] O. Durante,[89,90] D. D'Urso,[110,111] P.-A. Duverne,[39] I. Dvorkin,[153] S. E. Dwyer,[61] P. J. Easter,[6] M. Ebersold,[154] G. Eddolls,[65] B. Edelman,[54] T. B. Edo,[1,149] O. Edy,[148] A. Effler,[8] S. Eguchi,[119] J. Eichholz,[9] S. S. Eikenberry,[41] M. Eisenmann,[47] R. A. Eisenstein,[63] A. Ejlli,[17] Y. Enomoto,[29] L. Errico,[26,5] R. C. Essick,[123] H. Estellés,[135] D. Estevez,[155] Z. Etienne,[156] T. Etzel,[1] M. Evans,[63] T. M. Evans,[8] B. E. Ewing,[139] V. Fafone,[112,113,18] H. Fair,[55] S. Fairhurst,[17] X. Fan,[107] A. M. Farah,[123] S. Farinon,[78] B. Farr,[54] W. M. Farr,[103,104] N. W. Farrow,[6] E. J. Fauchon-Jones,[17] M. Favata,[157] M. Fays,[56,149] M. Fazio,[158] J. Feicht,[1] M. M. Fejer,[67] F. Feng,[35] E. Fenyvesi,[66,159] D. L. Ferguson,[100] A. Fernandez-Galiana,[63] I. Ferrante,[21,20] T. A. Ferreira,[16] F. Fidecaro,[21,20] P. Figura,[96] I. Fiori,[40] M. Fishbach,[15,123] R. P. Fisher,[7] J. M. Fishner,[63] R. Fittipaldi,[160,90] V. Fiumara,[161,90] R. Flaminio,[47,22]

E. Floden,[57] E. Flynn,[24] H. Fong,[30] J. A. Font,[116,162] B. Fornal,[163] P. W. F. Forsyth,[9] A. Franke,[146] S. Frasca,[91,46] F. Frasconi,[20] C. Frederick,[164] Z. Frei,[144] A. Freise,[165] R. Frey,[54] P. Fritschel,[63] V. V. Frolov,[8] G. G. Fronzé,[51] Y. Fujii,[166] Y. Fujikawa,[167] M. Fukunaga,[36] M. Fukushima,[23] P. Fulda,[41] M. Fyffe,[8] H. A. Gabbard,[65] B. U. Gadre,[99] S. M. Gaebel,[14] J. R. Gair,[99] J. Gais,[102] S. Galaudage,[6] R. Gamba,[13] D. Ganapathy,[63] A. Ganguly,[168] D. Gao,[169] S. G. Gaonkar,[3] B. Garaventa,[78,106] C. García-Núñez,[82] C. García-Quirós,[135] F. Garufi,[26,5] B. Gateley,[61] S. Gaudio,[34] V. Gayathri,[41] G. Ge,[169] G. Gemme,[78] A. Gennai,[20] J. George,[79] L. Gergely,[170] P. Gewecke,[146] S. Ghonge,[100] Abhirup. Ghosh,[99] Archisman Ghosh,[171] Shaon Ghosh,[28,157] Shrobana Ghosh,[17] Sourath Ghosh,[41] B. Giacomazzo,[58,59,60] L. Giacoppo,[91,46] J. A. Giaime,[2,8] K. D. Giardina,[8] D. R. Gibson,[82] C. Gier,[31] M. Giesler,[87] P. Giri,[20,21] F. Gissi,[75] J. Glanzer,[2] A. E. Gleckl,[24] P. Godwin,[139] E. Goetz,[172] R. Goetz,[41] N. Gohlke,[10,11] B. Goncharov,[6] G. González,[2] A. Gopakumar,[173] M. Gosselin,[40] R. Gouaty,[47] B. Grace,[9] A. Grado,[174,5] M. Granata,[150] V. Granata,[89] A. Grant,[65] S. Gras,[63] P. Grassia,[1] C. Gray,[61] R. Gray,[65] G. Greco,[68] A. C. Green,[41] R. Green,[17] A. M. Gretarsson,[34] E. M. Gretarsson,[34] D. Griffith,[1] W. Griffiths,[17] H. L. Griggs,[100] G. Grignani,[69,68] A. Grimaldi,[175,176] E. Grimes,[34] S. J. Grimm,[18,19] H. Grote,[17] S. Grunewald,[99] P. Gruning,[39] J. G. Guerrero,[24] G. M. Guidi,[84,85] A. R. Guimaraes,[2] G. Guixé,[62] H. K. Gulati,[73] H.-K. Guo,[163] Y. Guo,[48] Anchal Gupta,[1] Anuradha Gupta,[177] P. Gupta,[48,115] E. K. Gustafson,[1] R. Gustafson,[178] F. Guzman,[132] S. Ha,[179] L. Haegel,[35] A. Hagiwara,[36,180] S. Haino,[126] O. Halim,[181,33] E. D. Hall,[63] E. Z. Hamilton,[17] G. Hammond,[65] W.-B. Han,[182] M. Haney,[154] J. Hanks,[61] C. Hanna,[139] M. D. Hannam,[17] O. A. Hannuksela,[115,48,102] H. Hansen,[61] T. J. Hansen,[34] J. Hanson,[8] T. Harder,[86] T. Hardwick,[2] K. Haris,[48,115,168] J. Harms,[18,19] G. M. Harry,[183] I. W. Harry,[148] D. Hartwig,[146] K. Hasegawa,[36] B. Haskell,[74] R. K. Hasskew,[8] C.-J. Haster,[63] K. Hattori,[184] K. Haughian,[65] H. Hayakawa,[185] K. Hayama,[119] F. J. Hayes,[65] J. Healy,[117] A. Heidmann,[94] M. C. Heintze,[8] J. Heinze,[10,11] J. Heinzel,[186] H. Heitmann,[86] F. Hellman,[187] P. Hello,[39] A. F. Helmling-Cornell,[54] G. Hemming,[40] M. Hendry,[65] I. S. Heng,[65] E. Hennes,[48] J. Hennig,[10,11] M. H. Hennig,[10,11] F. Hernandez Vivanco,[6] M. Heurs,[10,11] S. Hild,[145,48] P. Hill,[31] Y. Himemoto,[188] A. S. Hines,[132] Y. Hiranuma,[189] N. Hirata,[22] E. Hirose,[36] S. Hochheim,[10,11] D. Hofman,[150] J. N. Hohmann,[146] A. M. Holgado,[25] N. A. Holland,[9] I. J. Hollows,[149] Z. J. Holmes,[76] K. Holt,[8] D. E. Holz,[123] Z. Hong,[190] P. Hopkins,[17] J. Hough,[65] E. J. Howell,[88] C. G. Hoy,[17] D. Hoyland,[14] A. Hreibi,[10,11] B. Hsieh,[36] Y. Hsu,[118] G-Z. Huang,[190] H-Y. Huang,[126] P. Huang,[169] Y-C. Huang,[122] Y.-J. Huang,[126] Y.-W. Huang,[63] M. T. Hübner,[6] A. D. Huddart,[133] E. A. Huerta,[25] B. Hughey,[34] D. C. Y. Hui,[191] V. Hui,[47] S. Husa,[135] S. H. Huttner,[65] R. Huxford,[139] T. Huynh-Dinh,[8] S. Ide,[192] B. Idzkowski,[96] A. Iess,[112,113] B. Ikenoue,[23] S. Imam,[190] K. Inayoshi,[193] H. Inchauspe,[41] C. Ingram,[76] Y. Inoue,[124] G. Intini,[91,46] K. Ioka,[194] M. Isi,[63] K. Isleif,[146] K. Ito,[195] Y. Itoh,[196,197] B. R. Iyer,[168] K. Izumi,[198] V. JaberianHamedan,[88] T. Jacqmin,[94] S. J. Jadhav,[199] S. P. Jadhav,[3] A. L. James,[17] A. Z. Jan,[117] K. Jani,[100] K. Janssens,[200] N. N. Janthalur,[199] P. Jaranowski,[201] D. Jariwala,[41] R. Jaume,[135] A. C. Jenkins,[130] C. Jeon,[202] M. Jeunon,[57] W. Jia,[63] J. Jiang,[41] H.-B. Jin,[203,204] G. R. Johns,[7] A. W. Jones,[88] D. I. Jones,[205] J. D. Jones,[61] P. Jones,[14] R. Jones,[65] R. J. G. Jonker,[48] L. Ju,[88] K. Jung,[179] P. Jung,[185] J. Junker,[10,11] K. Kaihotsu,[195] T. Kajita,[206] M. Kakizaki,[184] C. V. Kalaghatgi,[17] V. Kalogera,[15] B. Kamai,[1] M. Kamiizumi,[185] N. Kanda,[196,197] S. Kandhasamy,[3] G. Kang,[49] J. B. Kanner,[1] Y. Kao,[118] S. J. Kapadia,[168] D. P. Kapasi,[9] C. Karathanasis,[207] S. Karki,[80] R. Kashyap,[139] M. Kasprzack,[1] W. Kastaun,[10,11] S. Katsanevas,[40] E. Katsavounidis,[63] W. Katzman,[8] T. Kaur,[88] K. Kawabe,[61] K. Kawaguchi,[36] N. Kawai,[208] T. Kawasaki,[29] F. Kéfélian,[86] D. Keitel,[135] J. S. Key,[209] S. Khadka,[67] F. Y. Khalili,[81] I. Khan,[18,113] S. Khan,[17] E. A. Khazanov,[210] N. Khetan,[18,19] M. Khursheed,[79] N. Kijbunchoo,[9] C. Kim,[211,202] J. C. Kim,[212] J. Kim,[213] K. Kim,[214] W. S. Kim,[50] Y.-M. Kim,[179] C. Kimball,[15] N. Kimura,[180] P. J. King,[61] M. Kinley-Hanlon,[65] R. Kirchhoff,[10,11] J. S. Kissel,[61] N. Kita,[29] H. Kitazawa,[195] L. Kleybolte,[146] S. Klimenko,[41] A. M. Knee,[172] T. D. Knowles,[156] E. Knyazev,[63] P. Koch,[10,11] G. Koekoek,[48,145] Y. Kojima,[215] K. Kokeyama,[185] S. Koley,[48] P. Kolitsidou,[17] M. Kolstein,[207] K. Komori,[63,29] V. Kondrashov,[1] A. K. H. Kong,[122] A. Kontos,[216] N. Koper,[10,11] M. Korobko,[146] K. Kotake,[119] M. Kovalam,[88] D. B. Kozak,[1] C. Kozakai,[44] R. Kozu,[217] V. Kringel,[10,11] N. V. Krishnendu,[10,11] A. Królak,[218,219] G. Kuehn,[10,11] F. Kuei,[118] A. Kumar,[199] P. Kumar,[220] Rahul Kumar,[61] Rakesh Kumar,[73] J. Kume,[30] K. Kuns,[63] C. Kuo,[124] H-S. Kuo,[190] Y. Kuromiya,[195] S. Kuroyanagi,[221] K. Kusayanagi,[208] K. Kwak,[179] S. Kwang,[28] D. Laghi,[21,20] E. Lalande,[222] T. L. Lam,[102] A. Lamberts,[86,223] M. Landry,[61] B. B. Lane,[63] R. N. Lang,[63] J. Lange,[224,117] B. Lantz,[67] I. La Rosa,[47] A. Lartaux-Vollard,[39] P. D. Lasky,[6] M. Laxen,[8] A. Lazzarini,[1] C. Lazzaro,[70,71] P. Leaci,[91,46] S. Leavey,[10,11] Y. K. Lecoeuche,[61] H. K. Lee,[225] H. M. Lee,[214] H. W. Lee,[212] J. Lee,[128] K. Lee,[67] R. Lee,[122] J. Lehmann,[10,11] A. Lemaître,[226] E. Leon,[24] M. Leonardi,[22] N. Leroy,[39] N. Letendre,[47] Y. Levin,[6] J. N. Leviton,[178] A. K. Y. Li,[1] B. Li,[118] J. Li,[15] K. L. Li,[122] T. G. F. Li,[102] X. Li,[87] C-Y. Lin,[227] F-K. Lin,[126] F-L. Lin,[190] H. L. Lin,[124] L. C.-C. Lin,[179] F. Linde,[228,48] S. D. Linker,[77] J. N. Linley,[65] T. B. Littenberg,[229] G. C. Liu,[121] J. Liu,[10,11] K. Liu,[118] X. Liu,[28] M. Llorens-Monteagudo,[116] R. K. L. Lo,[1]

A. Lockwood,[230] M. L. Lollie,[2] L. T. London,[63] A. Longo,[231,232] D. Lopez,[154] M. Lorenzini,[112,113] V. Loriette,[233] M. Lormand,[8] G. Losurdo,[20] J. D. Lough,[10,11] C. O. Lousto,[117] G. Lovelace,[24] H. Lück,[10,11] D. Lumaca,[112,113] A. P. Lundgren,[148] L.-W. Luo,[126] R. Macas,[17] M. MacInnis,[63] D. M. Macleod,[17] I. A. O. MacMillan,[1] A. Macquet,[86] I. Magaña Hernandez,[28] F. Magaña-Sandoval,[41] C. Magazzù,[20] R. M. Magee,[139] R. Maggiore,[14] E. Majorana,[91,46] I. Maksimovic,[233] S. Maliakal,[1] A. Malik,[79] N. Man,[86] V. Mandic,[57] V. Mangano,[91,46] J. L. Mango,[234] G. L. Mansell,[61,63] M. Manske,[28] M. Mantovani,[40] M. Mapelli,[70,71] F. Marchesoni,[235,68] M. Marchio,[22] F. Marion,[47] Z. Mark,[87] S. Márka,[43] Z. Márka,[43] C. Markakis,[12] A. S. Markosyan,[67] A. Markowitz,[1] E. Maros,[1] A. Marquina,[137] S. Marsat,[35] F. Martelli,[84,85] I. W. Martin,[65] R. M. Martin,[157] M. Martinez,[207] V. Martinez,[27] K. Martinovic,[130] D. V. Martynov,[14] E. J. Marx,[63] H. Masalehdan,[146] K. Mason,[63] E. Massera,[149] A. Masserot,[47] T. J. Massinger,[63] M. Masso-Reid,[65] S. Mastrogiovanni,[35] A. Matas,[99] M. Mateu-Lucena,[135] F. Matichard,[1,63] M. Matiushechkina,[10,11] N. Mavalvala,[63] J. J. McCann,[88] R. McCarthy,[61] D. E. McClelland,[9] P. McClincy,[139] S. McCormick,[8] L. McCuller,[63] G. I. McGhee,[65] S. C. McGuire,[236] C. McIsaac,[148] J. McIver,[172] D. J. McManus,[9] T. McRae,[9] S. T. McWilliams,[156] D. Meacher,[28] M. Mehmet,[10,11] A. K. Mehta,[99] A. Melatos,[109] D. A. Melchor,[24] G. Mendell,[61] A. Menendez-Vazquez,[207] C. S. Menoni,[158] R. A. Mercer,[28] L. Mereni,[150] K. Merfeld,[54] E. L. Merilh,[61] J. D. Merritt,[54] M. Merzougui,[86] S. Meshkov,[1,†] C. Messenger,[65] C. Messick,[224] P. M. Meyers,[109] F. Meylahn,[10,11] A. Mhaske,[3] A. Miani,[175,176] H. Miao,[14] I. Michaloliakos,[41] C. Michel,[150] Y. Michimura,[29] H. Middleton,[109] L. Milano,[26] A. L. Miller,[95,41] M. Millhouse,[109] J. C. Mills,[17] E. Milotti,[181,33] M. C. Milovich-Goff,[77] O. Minazzoli,[86,237] Y. Minenkov,[113] N. Mio,[238] Ll. M. Mir,[207] A. Mishkin,[41] C. Mishra,[239] T. Mishra,[41] T. Mistry,[149] S. Mitra,[3] V. P. Mitrofanov,[81] G. Mitselmakher,[41] R. Mittleman,[63] O. Miyakawa,[185] A. Miyamoto,[196] Y. Miyazaki,[29] K. Miyo,[185] S. Miyoki,[185] Geoffrey Mo,[63] K. Mogushi,[80] S. R. P. Mohapatra,[63] S. R. Mohite,[28] I. Molina,[24] M. Molina-Ruiz,[187] M. Mondin,[77] M. Montani,[84,85] C. J. Moore,[14] D. Moraru,[61] F. Morawski,[74] A. More,[3] C. Moreno,[34] G. Moreno,[61] Y. Mori,[195] S. Morisaki,[30,36] Y. Moriwaki,[184] B. Mours,[155] C. M. Mow-Lowry,[14] S. Mozzon,[148] F. Muciaccia,[91,46] Arunava Mukherjee,[240,65] D. Mukherjee,[139] Soma Mukherjee,[141] Subroto Mukherjee,[73] N. Mukund,[10,11] A. Mullavey,[8] J. Munch,[76] E. A. Muñiz,[55] P. G. Murray,[65] R. Musenich,[78,106] S. L. Nadji,[10,11] K. Nagano,[198] S. Nagano,[241] A. Nagar,[51,242] K. Nakamura,[22] H. Nakano,[243] M. Nakano,[36] R. Nakashima,[208] Y. Nakayama,[184] I. Nardecchia,[112,113] T. Narikawa,[36] L. Naticchioni,[46] B. Nayak,[77] R. K. Nayak,[244] R. Negishi,[189] B. F. Neil,[88] J. Neilson,[75,90] G. Nelemans,[245] T. J. N. Nelson,[8] M. Nery,[10,11] A. Neunzert,[209] K. Y. Ng,[63] S. W. S. Ng,[76] C. Nguyen,[35] P. Nguyen,[54] T. Nguyen,[63] L. Nguyen Quynh,[246] W.-T. Ni,[203,169,247] S. A. Nichols,[2] A. Nishizawa,[30] S. Nissanke,[248,48] F. Nocera,[40] M. Noh,[172] M. Norman,[17] C. North,[17] S. Nozaki,[184] L. K. Nuttall,[148] J. Oberling,[61] B. D. O'Brien,[41] Y. Obuchi,[23] J. O'Dell,[133] W. Ogaki,[36] G. Oganesyan,[18,19] J. J. Oh,[50] K. Oh,[191] S. H. Oh,[50] M. Ohashi,[185] N. Ohishi,[44] M. Ohkawa,[167] F. Ohme,[10,11] H. Ohta,[30] M. A. Okada,[16] Y. Okutani,[192] K. Okutomi,[185] C. Olivetto,[40] K. Oohara,[189] C. Ooi,[29] R. Oram,[8] B. O'Reilly,[8] R. G. Ormiston,[57] N. D. Ormsby,[7] L. F. Ortega,[41] R. O'Shaughnessy,[117] E. O'Shea,[220] S. Oshino,[185] S. Ossokine,[99] C. Osthelder,[1] S. Otabe,[208] D. J. Ottaway,[76] H. Overmier,[8] A. E. Pace,[139] G. Pagano,[21,20] M. A. Page,[88] G. Pagliaroli,[18,19] A. Pai,[93] S. A. Pai,[79] J. R. Palamos,[54] O. Palashov,[210] C. Palomba,[46] K. Pan,[122] P. K. Panda,[199] H. Pang,[124] P. T. H. Pang,[48,115] C. Pankow,[15] F. Pannarale,[91,46] B. C. Pant,[79] F. Paoletti,[20] A. Paoli,[40] A. Paolone,[46,249] A. Parisi,[121] J. Park,[214] W. Parker,[8,236] D. Pascucci,[48] A. Pasqualetti,[40] R. Passaquieti,[21,20] D. Passuello,[20] M. Patel,[7] B. Patricelli,[40,20] E. Payne,[6] T. C. Pechsiri,[41] M. Pedraza,[1] M. Pegoraro,[71] A. Pele,[8] F. E. Peña Arellano,[185] S. Penn,[250] A. Perego,[175,176] A. Pereira,[27] T. Pereira,[251] C. J. Perez,[61] C. Périgois,[47] A. Perreca,[175,176] S. Perriès,[127] J. Petermann,[146] D. Petterson,[1] H. P. Pfeiffer,[99] K. A. Pham,[57] K. S. Phukon,[48,228,3] O. J. Piccinni,[46] M. Pichot,[86] M. Piendibene,[21,20] F. Piergiovanni,[84,85] L. Pierini,[91,46] V. Pierro,[75,90] G. Pillant,[40] F. Pilo,[20] L. Pinard,[150] I. M. Pinto,[75,90,252,253] B. J. Piotrzkowski,[28] K. Piotrzkowski,[95] M. Pirello,[61] M. Pitkin,[254] E. Placidi,[91,46] W. Plastino,[231,232] C. Pluchar,[132] R. Poggiani,[21,20] E. Polini,[47] D. Y. T. Pong,[102] S. Ponrathnam,[3] P. Popolizio,[40] E. K. Porter,[35] J. Powell,[255] M. Pracchia,[47] T. Pradier,[155] A. K. Prajapati,[73] K. Prasai,[67] R. Prasanna,[199] G. Pratten,[14] T. Prestegard,[28] M. Principe,[75,252,90] G. A. Prodi,[256,176] L. Prokhorov,[14] P. Prosposito,[112,113] L. Prudenzi,[99] A. Puecher,[48,115] M. Punturo,[68] F. Puosi,[20,21] P. Puppo,[46] M. Pürrer,[99] H. Qi,[17] V. Quetschke,[141] P. J. Quinonez,[34] R. Quitzow-James,[80] F. J. Raab,[61] G. Raaijmakers,[248,48] H. Radkins,[61] N. Radulesco,[86] P. Raffai,[144] S. X. Rail,[222] S. Raja,[79] C. Rajan,[79] K. E. Ramirez,[141] T. D. Ramirez,[24] A. Ramos-Buades,[99] J. Rana,[139] P. Rapagnani,[91,46] U. D. Rapol,[257] B. Ratto,[34] V. Raymond,[17] N. Raza,[172] M. Razzano,[21,20] J. Read,[24] L. A. Rees,[183] T. Regimbau,[47] L. Rei,[78] S. Reid,[31] D. H. Reitze,[1,41] P. Relton,[17] P. Rettegno,[258,51] F. Ricci,[91,46] C. J. Richardson,[34] J. W. Richardson,[1] L. Richardson,[132] P. M. Ricker,[25] G. Riemenschneider,[258,51] K. Riles,[178] M. Rizzo,[15] N. A. Robertson,[1,65] R. Robie,[1] F. Robinet,[39] A. Rocchi,[113] J. A. Rocha,[24] S. Rodriguez,[24] R. D. Rodriguez-Soto,[34] L. Rolland,[47] J. G. Rollins,[1] V. J. Roma,[54] M. Romanelli,[92] J. Romano,[259]

R. Romano,[4,5] C. L. Romel,[61] A. Romero,[207] I. M. Romero-Shaw,[6] J. H. Romie,[8] C. A. Rose,[28] D. Rosińska,[96] S. G. Rosofsky,[25] M. P. Ross,[230] S. Rowan,[65] S. J. Rowlinson,[14] Santosh Roy,[3] Soumen Roy,[260] D. Rozza,[110,111] P. Ruggi,[40] K. Ryan,[61] S. Sachdev,[139] T. Sadecki,[61] J. Sadiq,[147] N. Sago,[261] S. Saito,[23] Y. Saito,[185] K. Sakai,[262] Y. Sakai,[189] M. Sakellariadou,[130] Y. Sakuno,[119] O. S. Salafia,[60,59,58] L. Salconi,[40] M. Saleem,[263] F. Salemi,[175,176] A. Samajdar,[48,115] E. J. Sanchez,[1] J. H. Sanchez,[24] L. E. Sanchez,[1] N. Sanchis-Gual,[264] J. R. Sanders,[265] A. Sanuy,[62] T. R. Saravanan,[3] N. Sarin,[6] B. Sassolas,[150] H. Satari,[88] S. Sato,[266] T. Sato,[167] O. Sauter,[41,47] R. L. Savage,[61] V. Savant,[3] T. Sawada,[196] D. Sawant,[93] H. L. Sawant,[3] S. Sayah,[150] D. Schaetzl,[1] M. Scheel,[87] J. Scheuer,[15] A. Schindler-Tyka,[41] P. Schmidt,[14] R. Schnabel,[146] M. Schneewind,[10,11] R. M. S. Schofield,[54] A. Schönbeck,[146] B. W. Schulte,[10,11] B. F. Schutz,[17,10] E. Schwartz,[17] J. Scott,[65] S. M. Scott,[9] M. Seglar-Arroyo,[47] E. Seidel,[25] T. Sekiguchi,[30] Y. Sekiguchi,[267] D. Sellers,[8] A. S. Sengupta,[260] N. Sennett,[99] D. Sentenac,[40] E. G. Seo,[102] V. Sequino,[26,5] A. Sergeev,[210] Y. Setyawati,[10,11] T. Shaffer,[61] M. S. Shahriar,[15] B. Shams,[163] L. Shao,[193] S. Sharifi,[2] A. Sharma,[18,19] P. Sharma,[79] P. Shawhan,[98] N. S. Shcheblanov,[226] H. Shen,[25] S. Shibagaki,[119] M. Shikauchi,[30] R. Shimizu,[23] T. Shimoda,[29] K. Shimode,[185] R. Shink,[222] H. Shinkai,[268] T. Shishido,[45] A. Shoda,[22] D. H. Shoemaker,[63] D. M. Shoemaker,[224] K. Shukla,[187] S. ShyamSundar,[79] M. Sieniawska,[96] D. Sigg,[61] L. P. Singer,[105] D. Singh,[139] N. Singh,[96] A. Singha,[145,48] A. M. Sintes,[135] V. Sipala,[110,111] V. Skliris,[17] B. J. J. Slagmolen,[9] T. J. Slaven-Blair,[88] J. Smetana,[14] J. R. Smith,[24] R. J. E. Smith,[6] S. N. Somala,[269] K. Somiya,[208] E. J. Son,[50] K. Soni,[3] S. Soni,[2] B. Sorazu,[65] V. Sordini,[127] F. Sorrentino,[78] N. Sorrentino,[21,20] H. Sotani,[270] R. Soulard,[86] T. Souradeep,[257,3] E. Sowell,[138] V. Spagnuolo,[145,48] A. P. Spencer,[65] M. Spera,[70,71] A. K. Srivastava,[73] V. Srivastava,[55] K. Staats,[15] C. Stachie,[86] D. A. Steer,[35] J. Steinlechner,[145,48] S. Steinlechner,[145,48] D. J. Stops,[14] M. Stover,[164] K. A. Strain,[65] L. C. Strang,[109] G. Stratta,[271,85] A. Strunk,[61] R. Sturani,[251] A. L. Stuver,[101] J. Südbeck,[146] S. Sudhagar,[3] V. Sudhir,[63] R. Sugimoto,[272,198] H. G. Suh,[28] T. Z. Summerscales,[273] H. Sun,[88] L. Sun,[9,1] S. Sunil,[73] A. Sur,[74] J. Suresh,[30,36] P. J. Sutton,[17] Takamasa Suzuki,[167] Toshikazu Suzuki,[36] B. L. Swinkels,[48] M. J. Szczepańczyk,[41] P. Szewczyk,[96] M. Tacca,[48] H. Tagoshi,[36] S. C. Tait,[65] H. Takahashi,[274] R. Takahashi,[22] A. Takamori,[38] S. Takano,[29] H. Takeda,[29] M. Takeda,[196] C. Talbot,[1] H. Tanaka,[275] Kazuyuki Tanaka,[196] Kenta Tanaka,[275] Taiki Tanaka,[36] Takahiro Tanaka,[261] A. J. Tanasijczuk,[95] S. Tanioka,[22,45] D. B. Tanner,[41] D. Tao,[1] A. Tapia,[24] E. N. Tapia San Martin,[22] E. N. Tapia San Martin,[48] J. D. Tasson,[186] S. Telada,[276] R. Tenorio,[135] L. Terkowski,[146] M. Test,[28] M. P. Thirugnanasambandam,[3] M. Thomas,[8] P. Thomas,[61] J. E. Thompson,[17] S. R. Thondapu,[79] K. A. Thorne,[8] E. Thrane,[6] Shubhanshu Tiwari,[154] Srishti Tiwari,[173] V. Tiwari,[17] K. Toland,[65] A. E. Tolley,[148] T. Tomaru,[22] Y. Tomigami,[196] T. Tomura,[185] M. Tonelli,[21,20] A. Torres-Forné,[116] C. I. Torrie,[1] I. Tosta e Melo,[110,111] D. Töyrä,[9] A. Trapananti,[235,68] F. Travasso,[68,235] G. Traylor,[8] M. C. Tringali,[40] A. Tripathee,[178] L. Troiano,[277,90] A. Trovato,[35] L. Trozzo,[185] R. J. Trudeau,[1] D. S. Tsai,[118] D. Tsai,[118] K. W. Tsang,[48,278,115] T. Tsang,[102] J-S. Tsao,[190] M. Tse,[63] R. Tso,[87] K. Tsubono,[29] S. Tsuchida,[196] L. Tsukada,[30] D. Tsuna,[30] T. Tsutsui,[30] T. Tsuzuki,[23] M. Turconi,[86] D. Tuyenbayev,[126] A. S. Ubhi,[14] N. Uchikata,[36] T. Uchiyama,[185] R. P. Udall,[100,1] A. Ueda,[180] T. Uehara,[279,280] K. Ueno,[30] G. Ueshima,[274] D. Ugolini,[281] C. S. Unnikrishnan,[173] F. Uraguchi,[23] A. L. Urban,[2] T. Ushiba,[36] S. A. Usman,[123] A. C. Utina,[145,48] H. Vahlbruch,[10,11] G. Vajente,[1] A. Vajpeyi,[6] G. Valdes,[2] M. Valentini,[175,176] V. Valsan,[28] N. van Bakel,[48] M. van Beuzekom,[48] J. F. J. van den Brand,[145,97,48] C. Van Den Broeck,[115,48] N. van Remortel,[200] D. C. Vander-Hyde,[55] L. van der Schaaf,[48] J. V. van Heijningen,[88,95] M. H. P. M. van Putten,[282] M. Vardaro,[228,48] A. F. Vargas,[109] V. Varma,[87] M. Vasúth,[66] A. Vecchio,[14] G. Vedovato,[71] J. Veitch,[65] P. J. Veitch,[76] K. Venkateswara,[230] J. Venneberg,[10,11] G. Venugopalan,[1] D. Verkindt,[47] Y. Verma,[79] D. Veske,[43] F. Vetrano,[84] A. Viceré,[84,85] A. D. Viets,[234] V. Villa-Ortega,[147] J.-Y. Vinet,[86] S. Vitale,[63] T. Vo,[55] H. Vocca,[69,68] E. R. G. von Reis,[61] J. von Wrangel,[10,11] C. Vorvick,[61] S. P. Vyatchanin,[81] L. E. Wade,[164] M. Wade,[164] K. J. Wagner,[117] R. C. Walet,[48] M. Walker,[7] G. S. Wallace,[31] L. Wallace,[1] S. Walsh,[28] J. Wang,[169] J. Z. Wang,[178] W. H. Wang,[141] R. L. Ward,[9] J. Warner,[61] M. Was,[47] T. Washimi,[22] N. Y. Washington,[1] J. Watchi,[136] B. Weaver,[61] L. Wei,[10,11] M. Weinert,[10,11] A. J. Weinstein,[1] R. Weiss,[63] C. M. Weller,[230] F. Wellmann,[10,11] L. Wen,[88] P. Weßels,[10,11] J. W. Westhouse,[34] K. Wette,[9] J. T. Whelan,[117] D. D. White,[24] B. F. Whiting,[41] C. Whittle,[63] D. Wilken,[10,11] D. Williams,[65] M. J. Williams,[65] A. R. Williamson,[148] J. L. Willis,[1] B. Willke,[10,11] D. J. Wilson,[132] W. Winkler,[10,11] C. C. Wipf,[1] T. Wlodarczyk,[99] G. Woan,[65] J. Woehler,[10,11] J. K. Wofford,[117] I. C. F. Wong,[102] C. Wu,[122] D. S. Wu,[10,11] H. Wu,[122] S. Wu,[122] D. M. Wysocki,[28,117] L. Xiao,[1] W-R. Xu,[190] T. Yamada,[275] H. Yamamoto,[1] Kazuhiro Yamamoto,[184] Kohei Yamamoto,[275] T. Yamamoto,[185] K. Yamashita,[184] R. Yamazaki,[192] F. W. Yang,[163] L. Yang,[158] Yang Yang,[41] Yi Yang,[283] Z. Yang,[57] M. J. Yap,[9] D. W. Yeeles,[17] A. B. Yelikar,[117] M. Ying,[118] K. Yokogawa,[195] J. Yokoyama,[30,29] T. Yokozawa,[185] A. Yoon,[7] T. Yoshioka,[195] Hang Yu,[87] Haocun Yu,[63] H. Yuzurihara,[36] A. Zadrożny,[219] M. Zanolin,[34] S. Zeidler,[284] T. Zelenova,[40] J.-P. Zendri,[71] M. Zevin,[15] M. Zhan,[169] H. Zhang,[190] J. Zhang,[88] L. Zhang,[1]

R. Zhang,[41] T. Zhang,[14] C. Zhao,[88] G. Zhao,[136] Yue Zhao,[163] Yuhang Zhao,[22] Z. Zhou,[15] X. J. Zhu,[6] Z.-H. Zhu,[108] M. E. Zucker,[1,63] and J. Zweizig[1]

(LIGO Scientific Collaboration, Virgo Collaboration, and KAGRA Collaboration)

[1]*LIGO Laboratory, California Institute of Technology, Pasadena, California 91125, USA*
[2]*Louisiana State University, Baton Rouge, Louisiana 70803, USA*
[3]*Inter-University Centre for Astronomy and Astrophysics, Pune 411007, India*
[4]*Dipartimento di Farmacia, Università di Salerno, I-84084 Fisciano, Salerno, Italy*
[5]*INFN, Sezione di Napoli, Complesso Universitario di Monte S. Angelo, I-80126 Napoli, Italy*
[6]*OzGrav, School of Physics & Astronomy, Monash University, Clayton 3800, Victoria, Australia*
[7]*Christopher Newport University, Newport News, Virginia 23606, USA*
[8]*LIGO Livingston Observatory, Livingston, Louisiana 70754, USA*
[9]*OzGrav, Australian National University, Canberra, Australian Capital Territory 0200, Australia*
[10]*Max Planck Institute for Gravitational Physics (Albert Einstein Institute), D-30167 Hannover, Germany*
[11]*Leibniz Universität Hannover, D-30167 Hannover, Germany*
[12]*University of Cambridge, Cambridge CB2 1TN, United Kingdom*
[13]*Theoretisch-Physikalisches Institut, Friedrich-Schiller-Universität Jena, D-07743 Jena, Germany*
[14]*University of Birmingham, Birmingham B15 2TT, United Kingdom*
[15]*Center for Interdisciplinary Exploration & Research in Astrophysics (CIERA), Northwestern University, Evanston, Illinois 60208, USA*
[16]*Instituto Nacional de Pesquisas Espaciais, 12227-010 São José dos Campos, São Paulo, Brazil*
[17]*Gravity Exploration Institute, Cardiff University, Cardiff CF24 3AA, United Kingdom*
[18]*Gran Sasso Science Institute (GSSI), I-67100 L'Aquila, Italy*
[19]*INFN, Laboratori Nazionali del Gran Sasso, I-67100 Assergi, Italy*
[20]*INFN, Sezione di Pisa, I-56127 Pisa, Italy*
[21]*Università di Pisa, I-56127 Pisa, Italy*
[22]*Gravitational Wave Science Project, National Astronomical Observatory of Japan (NAOJ), Mitaka City, Tokyo 181-8588, Japan*
[23]*Advanced Technology Center, National Astronomical Observatory of Japan (NAOJ), Mitaka City, Tokyo 181-8588, Japan*
[24]*California State University Fullerton, Fullerton, California 92831, USA*
[25]*NCSA, University of Illinois at Urbana-Champaign, Urbana, Illinois 61801, USA*
[26]*Università di Napoli "Federico II", Complesso Universitario di Monte S.Angelo, I-80126 Napoli, Italy*
[27]*Université de Lyon, Université Claude Bernard Lyon 1, CNRS, Institut Lumière Matière, F-69622 Villeurbanne, France*
[28]*University of Wisconsin-Milwaukee, Milwaukee, Wisconsin 53201, USA*
[29]*Department of Physics, The University of Tokyo, Bunkyo-ku, Tokyo 113-0033, Japan*
[30]*Research Center for the Early Universe (RESCEU), The University of Tokyo, Bunkyo-ku, Tokyo 113-0033, Japan*
[31]*SUPA, University of Strathclyde, Glasgow G1 1XQ, United Kingdom*
[32]*Dipartimento di Matematica e Informatica, Università di Udine, I-33100 Udine, Italy*
[33]*INFN, Sezione di Trieste, I-34127 Trieste, Italy*
[34]*Embry-Riddle Aeronautical University, Prescott, Arizona 86301, USA*
[35]*Université de Paris, CNRS, Astroparticule et Cosmologie, F-75006 Paris, France*
[36]*Institute for Cosmic Ray Research (ICRR), KAGRA Observatory, The University of Tokyo, Kashiwa City, Chiba 277-8582, Japan*
[37]*Accelerator Laboratory, High Energy Accelerator Research Organization (KEK), Tsukuba City, Ibaraki 305-0801, Japan*
[38]*Earthquake Research Institute, The University of Tokyo, Bunkyo-ku, Tokyo 113-0032, Japan*
[39]*Université Paris-Saclay, CNRS/IN2P3, IJCLab, 91405 Orsay, France*
[40]*European Gravitational Observatory (EGO), I-56021 Cascina, Pisa, Italy*
[41]*University of Florida, Gainesville, Florida 32611, USA*
[42]*Department of Mathematics and Physics, Hirosaki University, Hirosaki City, Aomori 036-8561, Japan*
[43]*Columbia University, New York, New York 10027, USA*
[44]*Kamioka Branch, National Astronomical Observatory of Japan (NAOJ), Kamioka-cho, Hida City, Gifu 506-1205, Japan*
[45]*The Graduate University for Advanced Studies (SOKENDAI), Mitaka City, Tokyo 181-8588, Japan*
[46]*INFN, Sezione di Roma, I-00185 Roma, Italy*

[47]*Univ. Grenoble Alpes, Laboratoire d'Annecy de Physique des Particules (LAPP),*
Université Savoie Mont Blanc, CNRS/IN2P3, F-74941 Annecy, France
[48]*Nikhef, Science Park 105, 1098 XG Amsterdam, Netherlands*
[49]*Korea Institute of Science and Technology Information (KISTI), Yuseong-gu, Daejeon 34141, Korea*
[50]*National Institute for Mathematical Sciences, Daejeon 34047, South Korea*
[51]*INFN Sezione di Torino, I-10125 Torino, Italy*
[52]*International College, Osaka University, Toyonaka City, Osaka 560-0043, Japan*
[53]*School of High Energy Accelerator Science, The Graduate University for Advanced Studies*
(SOKENDAI), Tsukuba City, Ibaraki 305-0801, Japan
[54]*University of Oregon, Eugene, Oregon 97403, USA*
[55]*Syracuse University, Syracuse, New York 13244, USA*
[56]*Université de Liège, B-4000 Liège, Belgium*
[57]*University of Minnesota, Minneapolis, Minnesota 55455, USA*
[58]*Università degli Studi di Milano-Bicocca, I-20126 Milano, Italy*
[59]*INFN, Sezione di Milano-Bicocca, I-20126 Milano, Italy*
[60]*INAF, Osservatorio Astronomico di Brera sede di Merate, I-23807 Merate, Lecco, Italy*
[61]*LIGO Hanford Observatory, Richland, Washington 99352, USA*
[62]*Institut de Ciències del Cosmos, Universitat de Barcelona,*
C/ Martí i Franquès 1, Barcelona 08028, Spain
[63]*LIGO Laboratory, Massachusetts Institute of Technology, Cambridge, Massachusetts 02139, USA*
[64]*Dipartimento di Medicina, "Chirurgia e Odontoiatria Scuola Medica Salernitana",*
Università di Salerno, I-84081 Baronissi, Salerno, Italy
[65]*SUPA, University of Glasgow, Glasgow G12 8QQ, United Kingdom*
[66]*Wigner RCP, RMKI, H-1121 Budapest, Konkoly Thege Miklós út 29-33, Hungary*
[67]*Stanford University, Stanford, California 94305, USA*
[68]*INFN, Sezione di Perugia, I-06123 Perugia, Italy*
[69]*Università di Perugia, I-06123 Perugia, Italy*
[70]*Università di Padova, Dipartimento di Fisica e Astronomia, I-35131 Padova, Italy*
[71]*INFN, Sezione di Padova, I-35131 Padova, Italy*
[72]*Montana State University, Bozeman, Montana 59717, USA*
[73]*Institute for Plasma Research, Bhat, Gandhinagar 382428, India*
[74]*Nicolaus Copernicus Astronomical Center, Polish Academy of Sciences, 00-716 Warsaw, Poland*
[75]*Dipartimento di Ingegneria, Università del Sannio, I-82100 Benevento, Italy*
[76]*OzGrav, University of Adelaide, Adelaide, South Australia 5005, Australia*
[77]*California State University, Los Angeles, 5151 State University Dr, Los Angeles, California 90032, USA*
[78]*INFN, Sezione di Genova, I-16146 Genova, Italy*
[79]*RRCAT, Indore, Madhya Pradesh 452013, India*
[80]*Missouri University of Science and Technology, Rolla, Missouri 65409, USA*
[81]*Faculty of Physics, Lomonosov Moscow State University, Moscow 119991, Russia*
[82]*SUPA, University of the West of Scotland, Paisley PA1 2BE, United Kingdom*
[83]*Bar-Ilan University, Ramat Gan 5290002, Israel*
[84]*Università degli Studi di Urbino "Carlo Bo", I-61029 Urbino, Italy*
[85]*INFN, Sezione di Firenze, I-50019 Sesto Fiorentino, Firenze, Italy*
[86]*Artemis, Université Côte d'Azur, Observatoire Côte d'Azur, CNRS, F-06304 Nice, France*
[87]*CaRT, California Institute of Technology, Pasadena, California 91125, USA*
[88]*OzGrav, University of Western Australia, Crawley, Western Australia 6009, Australia*
[89]*Dipartimento di Fisica "E.R. Caianiello", Università di Salerno, I-84084 Fisciano, Salerno, Italy*
[90]*INFN, Sezione di Napoli, Gruppo Collegato di Salerno, Complesso Universitario di Monte S. Angelo,*
I-80126 Napoli, Italy
[91]*Università di Roma "La Sapienza", I-00185 Roma, Italy*
[92]*Univ Rennes, CNRS, Institut FOTON - UMR6082, F-3500 Rennes, France*
[93]*Indian Institute of Technology Bombay, Powai, Mumbai 400 076, India*
[94]*Laboratoire Kastler Brossel, Sorbonne Université, CNRS, ENS-Université PSL, Collège de France,*
F-75005 Paris, France
[95]*Université catholique de Louvain, B-1348 Louvain-la-Neuve, Belgium*
[96]*Astronomical Observatory Warsaw University, 00-478 Warsaw, Poland*
[97]*VU University Amsterdam, 1081 HV Amsterdam, Netherlands*
[98]*University of Maryland, College Park, Maryland 20742, USA*
[99]*Max Planck Institute for Gravitational Physics (Albert Einstein Institute), D-14476 Potsdam, Germany*
[100]*School of Physics, Georgia Institute of Technology, Atlanta, Georgia 30332, USA*

[101]*Villanova University, 800 Lancaster Ave, Villanova, Pennsylvania 19085, USA*

[102]*Faculty of Science, Department of Physics, The Chinese University of Hong Kong,*
Shatin, N.T., Hong Kong

[103]*Stony Brook University, Stony Brook, New York 11794, USA*

[104]*Center for Computational Astrophysics, Flatiron Institute, New York, New York 10010, USA*

[105]*NASA Goddard Space Flight Center, Greenbelt, Maryland 20771, USA*

[106]*Dipartimento di Fisica, Università degli Studi di Genova, I-16146 Genova, Italy*

[107]*Tsinghua University, Beijing 100084, China*

[108]*Department of Astronomy, Beijing Normal University, Beijing 100875, China*

[109]*OzGrav, University of Melbourne, Parkville, Victoria 3010, Australia*

[110]*Università degli Studi di Sassari, I-07100 Sassari, Italy*

[111]*INFN, Laboratori Nazionali del Sud, I-95125 Catania, Italy*

[112]*Università di Roma Tor Vergata, I-00133 Roma, Italy*

[113]*INFN, Sezione di Roma Tor Vergata, I-00133 Roma, Italy*

[114]*University of Sannio at Benevento, I-82100 Benevento, Italy and INFN, Sezione di Napoli,*
I-80100 Napoli, Italy

[115]*Institute for Gravitational and Subatomic Physics (GRASP), Utrecht University,*
Princetonplein 1, 3584 CC Utrecht, Netherlands

[116]*Departamento de Astronomía y Astrofísica, Universitat de València,*
E-46100 Burjassot, València, Spain

[117]*Rochester Institute of Technology, Rochester, New York 14623, USA*

[118]*National Tsing Hua University, Hsinchu City, 30013 Taiwan, Republic of China*

[119]*Department of Applied Physics, Fukuoka University, Jonan, Fukuoka City, Fukuoka 814-0180, Japan*

[120]*OzGrav, Charles Sturt University, Wagga Wagga, New South Wales 2678, Australia*

[121]*Department of Physics, Tamkang University, Danshui Dist., New Taipei City 25137, Taiwan*

[122]*Department of Physics and Institute of Astronomy, National Tsing Hua University,*
Hsinchu 30013, Taiwan

[123]*University of Chicago, Chicago, Illinois 60637, USA*

[124]*Department of Physics, Center for High Energy and High Field Physics, National Central University,*
Zhongli District, Taoyuan City 32001, Taiwan

[125]*Dipartimento di Ingegneria Industriale (DIIN), Università di Salerno, I-84084 Fisciano, Salerno, Italy*

[126]*Institute of Physics, Academia Sinica, Nankang, Taipei 11529, Taiwan*

[127]*Institut de Physique des 2 Infinis de Lyon (IP2I), CNRS/IN2P3, Université de Lyon,*
Université Claude Bernard Lyon 1, F-69622 Villeurbanne, France

[128]*Seoul National University, Seoul 08826, South Korea*

[129]*Pusan National University, Busan 46241, South Korea*

[130]*King's College London, University of London, London WC2R 2LS, United Kingdom*

[131]*INAF, Osservatorio Astronomico di Padova, I-35122 Padova, Italy*

[132]*University of Arizona, Tucson, Arizona 85721, USA*

[133]*Rutherford Appleton Laboratory, Didcot OX11 0DE, United Kingdom*

[134]*Université libre de Bruxelles, Avenue Franklin Roosevelt 50 - 1050 Bruxelles, Belgium*

[135]*Universitat de les Illes Balears, IAC3—IEEC, E-07122 Palma de Mallorca, Spain*

[136]*Université Libre de Bruxelles, Brussels 1050, Belgium*

[137]*Departamento de Matemáticas, Universitat de València, E-46100 Burjassot, València, Spain*

[138]*Texas Tech University, Lubbock, Texas 79409, USA*

[139]*The Pennsylvania State University, University Park, Pennsylvania 16802, USA*

[140]*University of Rhode Island, Kingston, Rhode Island 02881, USA*

[141]*The University of Texas Rio Grande Valley, Brownsville, Texas 78520, USA*

[142]*Bellevue College, Bellevue, Washington 98007, USA*

[143]*Scuola Normale Superiore, Piazza dei Cavalieri, 7 - 56126 Pisa, Italy*

[144]*MTA-ELTE Astrophysics Research Group, Institute of Physics, Eötvös University,*
Budapest 1117, Hungary

[145]*Maastricht University, 6200 MD, Maastricht, Netherlands*

[146]*Universität Hamburg, D-22761 Hamburg, Germany*

[147]*IGFAE, Campus Sur, Universidade de Santiago de Compostela, 15782 Spain*

[148]*University of Portsmouth, Portsmouth PO1 3FX, United Kingdom*

[149]*The University of Sheffield, Sheffield S10 2TN, United Kingdom*

[150]*Laboratoire des Matériaux Avancés (LMA), Institut de Physique des 2 Infinis (IP2I) de Lyon,*
CNRS/IN2P3, Université de Lyon, Université Claude Bernard Lyon 1, F-69622 Villeurbanne, France

[151]*Dipartimento di Scienze Matematiche, Fisiche e Informatiche, Università di Parma, I-43124 Parma, Italy*

[152]*INFN, Sezione di Milano Bicocca, Gruppo Collegato di Parma, I-43124 Parma, Italy*

[153]*Institut dAstrophysique de Paris, Sorbonne Université & CNRS, UMR 7095, 98 bis bd Arago, F-75014 Paris, France*

[154]*Physik-Institut, University of Zurich, Winterthurerstrasse 190, 8057 Zurich, Switzerland*

[155]*Université de Strasbourg, CNRS, IPHC UMR 7178, F-67000 Strasbourg, France*

[156]*West Virginia University, Morgantown, West Virginia 26506, USA*

[157]*Montclair State University, Montclair, New Jersey 07043, USA*

[158]*Colorado State University, Fort Collins, Colorado 80523, USA*

[159]*Institute for Nuclear Research, Hungarian Academy of Sciences, Bem t'er 18/c, H-4026 Debrecen, Hungary*

[160]*CNR-SPIN, c/o Università di Salerno, I-84084 Fisciano, Salerno, Italy*

[161]*Scuola di Ingegneria, Università della Basilicata, I-85100 Potenza, Italy*

[162]*Observatori Astronòmic, Universitat de València, E-46980 Paterna, València, Spain*

[163]*The University of Utah, Salt Lake City, Utah 84112, USA*

[164]*Kenyon College, Gambier, Ohio 43022, USA*

[165]*Vrije Universiteit Amsterdam, 1081 HV, Amsterdam, Netherlands*

[166]*Department of Astronomy, The University of Tokyo, Mitaka City, Tokyo 181-8588, Japan*

[167]*Faculty of Engineering, Niigata University, Nishi-ku, Niigata City, Niigata 950-2181, Japan*

[168]*International Centre for Theoretical Sciences, Tata Institute of Fundamental Research, Bengaluru 560089, India*

[169]*State Key Laboratory of Magnetic Resonance and Atomic and Molecular Physics, Innovation Academy for Precision Measurement Science and Technology (APM), Chinese Academy of Sciences, Xiao Hong Shan, Wuhan 430071, China*

[170]*University of Szeged, Dóm tér 9, Szeged 6720, Hungary*

[171]*Universiteit Gent, B-9000 Gent, Belgium*

[172]*University of British Columbia, Vancouver, BC V6T 1Z4, Canada*

[173]*Tata Institute of Fundamental Research, Mumbai 400005, India*

[174]*INAF, Osservatorio Astronomico di Capodimonte, I-80131 Napoli, Italy*

[175]*Università di Trento, Dipartimento di Fisica, I-38123 Povo, Trento, Italy*

[176]*INFN, Trento Institute for Fundamental Physics and Applications, I-38123 Povo, Trento, Italy*

[177]*The University of Mississippi, University, Mississippi 38677, USA*

[178]*University of Michigan, Ann Arbor, Michigan 48109, USA*

[179]*Department of Physics, School of Natural Science, Ulsan National Institute of Science and Technology (UNIST), Ulju-gun, Ulsan 44919, Korea*

[180]*Applied Research Laboratory, High Energy Accelerator Research Organization (KEK), Tsukuba City, Ibaraki 305-0801, Japan*

[181]*Dipartimento di Fisica, Università di Trieste, I-34127 Trieste, Italy*

[182]*Shanghai Astronomical Observatory, Chinese Academy of Sciences, Shanghai 200030, China*

[183]*American University, Washington, D.C. 20016, USA*

[184]*Faculty of Science, University of Toyama, Toyama City, Toyama 930-8555, Japan*

[185]*Institute for Cosmic Ray Research (ICRR), KAGRA Observatory, The University of Tokyo, Kamioka-cho, Hida City, Gifu 506-1205, Japan*

[186]*Carleton College, Northfield, Minnesota 55057, USA*

[187]*University of California, Berkeley, California 94720, USA*

[188]*College of Industrial Technology, Nihon University, Narashino City, Chiba 275-8575, Japan*

[189]*Graduate School of Science and Technology, Niigata University, Nishi-ku, Niigata City, Niigata 950-2181, Japan*

[190]*Department of Physics, National Taiwan Normal University, sec. IV, Taipei 116, Taiwan*

[191]*Astronomy & Space Science, Chungnam National University, Yuseong-gu, Daejeon 34134, Korea, Korea*

[192]*Department of Physics and Mathematics, Aoyama Gakuin University, Sagamihara City, Kanagawa 252-5258, Japan*

[193]*Kavli Institute for Astronomy and Astrophysics, Peking University, Haidian District, Beijing 100871, China*

[194]*Yukawa Institute for Theoretical Physics (YITP), Kyoto University, Sakyou-ku, Kyoto City, Kyoto 606-8502, Japan*

[195]*Graduate School of Science and Engineering, University of Toyama, Toyama City, Toyama 930-8555, Japan*

[196]*Department of Physics, Graduate School of Science, Osaka City University, Sumiyoshi-ku, Osaka City, Osaka 558-8585, Japan*

[197]*Nambu Yoichiro Institute of Theoretical and Experimental Physics (NITEP), Osaka City University, Sumiyoshi-ku, Osaka City, Osaka 558-8585, Japan*

[198]*Institute of Space and Astronautical Science (JAXA), Chuo-ku, Sagamihara City, Kanagawa 252-0222, Japan*

[199]*Directorate of Construction, Services & Estate Management, Mumbai 400094 India*

[200]*Universiteit Antwerpen, Prinsstraat 13, 2000 Antwerpen, Belgium*

[201]*University of Białystok, 15-424 Białystok, Poland*

[202]*Department of Physics, Ewha Womans University, Seodaemun-gu, Seoul 03760, Korea*

[203]*National Astronomical Observatories, Chinese Academic of Sciences, Chaoyang District, Beijing, China*

[204]*School of Astronomy and Space Science, University of Chinese Academy of Sciences, Chaoyang District, Beijing, China*

[205]*University of Southampton, Southampton SO17 1BJ, United Kingdom*

[206]*Institute for Cosmic Ray Research (ICRR), The University of Tokyo, Kashiwa City, Chiba 277-8582, Japan*

[207]*Institut de Física d'Altes Energies (IFAE), Barcelona Institute of Science and Technology, and ICREA, E-08193 Barcelona, Spain*

[208]*Graduate School of Science and Technology, Tokyo Institute of Technology, Meguro-ku, Tokyo 152-8551, Japan*

[209]*University of Washington Bothell, Bothell, Washington 98011, USA*

[210]*Institute of Applied Physics, Nizhny Novgorod, 603950, Russia*

[211]*Ewha Womans University, Seoul 03760, South Korea*

[212]*Inje University Gimhae, South Gyeongsang 50834, South Korea*

[213]*Department of Physics, Myongji University, Yongin 17058, Korea*

[214]*Korea Astronomy and Space Science Institute (KASI), Yuseong-gu, Daejeon 34055, Korea*

[215]*Department of Physical Science, Hiroshima University, Higashihiroshima City, Hiroshima 903-0213, Japan*

[216]*Bard College, 30 Campus Rd, Annandale-On-Hudson, New York 12504, USA*

[217]*Institute for Cosmic Ray Research (ICRR), Research Center for Cosmic Neutrinos (RCCN), The University of Tokyo, Kamioka-cho, Hida City, Gifu 506-1205, Japan*

[218]*Institute of Mathematics, Polish Academy of Sciences, 00656 Warsaw, Poland*

[219]*National Center for Nuclear Research, 05-400 Świerk-Otwock, Poland*

[220]*Cornell University, Ithaca, New York 14850, USA*

[221]*Institute for Advanced Research, Nagoya University, Furocho, Chikusa-ku, Nagoya City, Aichi 464-8602, Japan*

[222]*Université de Montréal/Polytechnique, Montreal, Quebec H3T 1J4, Canada*

[223]*Laboratoire Lagrange, Université Côte d'Azur, Observatoire Côte d'Azur, CNRS, F-06304 Nice, France*

[224]*Department of Physics, University of Texas, Austin, Texas 78712, USA*

[225]*Department of Physics, Hanyang University, Seoul 04763, Korea*

[226]*NAVIER, École des Ponts, Univ Gustave Eiffel, CNRS, Marne-la-Vallée, France*

[227]*National Center for High-performance computing, National Applied Research Laboratories, Hsinchu Science Park, Hsinchu City 30076, Taiwan*

[228]*Institute for High-Energy Physics, University of Amsterdam, Science Park 904, 1098 XH Amsterdam, Netherlands*

[229]*NASA Marshall Space Flight Center, Huntsville, Alabama 35811, USA*

[230]*University of Washington, Seattle, Washington 98195, USA*

[231]*Dipartimento di Matematica e Fisica, Università degli Studi Roma Tre, I-00146 Roma, Italy*

[232]*INFN, Sezione di Roma Tre, I-00146 Roma, Italy*

[233]*ESPCI, CNRS, F-75005 Paris, France*

[234]*Concordia University Wisconsin, Mequon, Wisconsin 53097, USA*

[235]*Università di Camerino, Dipartimento di Fisica, I-62032 Camerino, Italy*

[236]*Southern University and A&M College, Baton Rouge, Louisiana 70813, USA*

[237]*Centre Scientifique de Monaco, 8 quai Antoine Ier, MC-98000, Monaco*

[238]*Institute for Photon Science and Technology, The University of Tokyo, Bunkyo-ku, Tokyo 113-8656, Japan*

[239]*Indian Institute of Technology Madras, Chennai 600036, India*

[240]*Saha Institute of Nuclear Physics, Bidhannagar, West Bengal 700064, India*

[241]The Applied Electromagnetic Research Institute, National Institute of Information and Communications Technology (NICT), Koganei City, Tokyo 184-8795, Japan

[242]Institut des Hautes Etudes Scientifiques, F-91440 Bures-sur-Yvette, France

[243]Faculty of Law, Ryukoku University, Fushimi-ku, Kyoto City, Kyoto 612-8577, Japan

[244]Indian Institute of Science Education and Research, Kolkata, Mohanpur, West Bengal 741252, India

[245]Department of Astrophysics/IMAPP, Radboud University Nijmegen, P.O. Box 9010, 6500 GL Nijmegen, Netherlands

[246]Department of Physics, University of Notre Dame, Notre Dame, Indiana 46556, USA

[247]Department of Physics, National Tsing Hua University, Hsinchu 30013, Taiwan

[248]GRAPPA, Anton Pannekoek Institute for Astronomy and Institute for High-Energy Physics, University of Amsterdam, Science Park 904, 1098 XH Amsterdam, Netherlands

[249]Consiglio Nazionale delle Ricerche - Istituto dei Sistemi Complessi, Piazzale Aldo Moro 5, I-00185 Roma, Italy

[250]Hobart and William Smith Colleges, Geneva, New York 14456, USA

[251]International Institute of Physics, Universidade Federal do Rio Grande do Norte, Natal RN 59078-970, Brazil

[252]Museo Storico della Fisica e Centro Studi e Ricerche "Enrico Fermi", I-00184 Roma, Italy

[253]Department of Engineering, University of Sannio, Benevento 82100, Italy

[254]Lancaster University, Lancaster LA1 4YW, United Kingdom

[255]OzGrav, Swinburne University of Technology, Hawthorn VIC 3122, Australia

[256]Università di Trento, Dipartimento di Matematica, I-38123 Povo, Trento, Italy

[257]Indian Institute of Science Education and Research, Pune, Maharashtra 411008, India

[258]Dipartimento di Fisica, Università degli Studi di Torino, I-10125 Torino, Italy

[259]Department of Physics and Astronomy, Texas Tech University, Box 41051, Lubbock, Texas 79409-1051, USA

[260]Indian Institute of Technology, Palaj, Gandhinagar, Gujarat 382355, India

[261]Department of Physics, Kyoto University, Sakyou-ku, Kyoto City, Kyoto 606-8502, Japan

[262]Department of Electronic Control Engineering, National Institute of Technology, Nagaoka College, Nagaoka City, Niigata 940-8532, Japan

[263]Chennai Mathematical Institute, Chennai 603103, India

[264]Centro de Astrofísica e Gravitação (CENTRA), Departamento de Física, Instituto Superior Técnico, Universidade de Lisboa, 1049-001 Lisboa, Portugal

[265]Marquette University, 11420 W. Clybourn Street, Milwaukee, Wisconsin 53233, USA

[266]Graduate School of Science and Engineering, Hosei University, Koganei City, Tokyo 184-8584, Japan

[267]Faculty of Science, Toho University, Funabashi City, Chiba 274-8510, Japan

[268]Faculty of Information Science and Technology, Osaka Institute of Technology, Hirakata City, Osaka 573-0196, Japan

[269]Indian Institute of Technology Hyderabad, Sangareddy, Khandi, Telangana 502285, India

[270]iTHEMS (Interdisciplinary Theoretical and Mathematical Sciences Program), The Institute of Physical and Chemical Research (RIKEN), Wako, Saitama 351-0198, Japan

[271]INAF, Osservatorio di Astrofisica e Scienza dello Spazio, I-40129 Bologna, Italy

[272]Department of Space and Astronautical Science, The Graduate University for Advanced Studies (SOKENDAI), Sagamihara, Kanagawa 252-5210, Japan

[273]Andrews University, Berrien Springs, Michigan 49104, USA

[274]Department of Information and Management Systems Engineering, Nagaoka University of Technology, Nagaoka City, Niigata 940-2188, Japan

[275]Institute for Cosmic Ray Research (ICRR), Research Center for Cosmic Neutrinos (RCCN), The University of Tokyo, Kashiwa City, Chiba 277-8582, Japan

[276]National Metrology Institute of Japan, National Institute of Advanced Industrial Science and Technology, Tsukuba City, Ibaraki 305-8568, Japan

[277]Dipartimento di Scienze Aziendali—Management and Innovation Systems (DISA-MIS), Università di Salerno, I-84084 Fisciano, Salerno, Italy

[278]Van Swinderen Institute for Particle Physics and Gravity, University of Groningen, Nijenborgh 4, 9747 AG Groningen, Netherlands

[279]Department of Communications Engineering, National Defense Academy of Japan, Yokosuka City, Kanagawa 239-8686, Japan

[280]Department of Physics, University of Florida, Gainesville, Florida 32611, USA

[281]Trinity University, San Antonio, Texas 78212, USA

[282]Department of Physics and Astronomy, Sejong University, Gwangjin-gu, Seoul 143-747, Korea
[283]Department of Electrophysics, National Chiao Tung University, Hsinchu 30010, Taiwan
[284]Department of Physics, Rikkyo University, Toshima-ku, Tokyo 171-8501, Japan

[†]Deceased, August 2020.